

# Light dark Higgs boson in minimal sub-GeV dark matter scenarios

Luc Darmé,<sup>1,a</sup> Soumya Rao,<sup>1,b</sup> and Leszek Roszkowski<sup>1,2,c</sup>

<sup>1</sup> *National Centre for Nuclear Research,  
Hoża 69, 00-681 Warsaw, Poland*

<sup>2</sup> *Consortium for Fundamental Physics, Department of Physics and Astronomy,  
University of Sheffield, Sheffield S3 7RH, United Kingdom*

## Abstract

Minimal scenarios with light (sub-GeV) dark matter whose relic density is obtained from thermal freeze-out must include new light mediators. In particular, a very well-motivated case is that of a new “dark” massive vector gauge boson mediator. The mass term for such mediator is most naturally obtained by a “dark Higgs mechanism” which leads to the presence of an often long-lived dark Higgs boson whose mass scale is the same as that of the mediator. We study the phenomenology and experimental constraints on two minimal, self-consistent dark sectors that include such a light dark Higgs boson. In one the dark matter is a pseudo-Dirac fermion, in the other a complex scalar. We find that the constraints from BBN and CMB are considerably relaxed in the framework of such minimal dark sectors. We present detection prospects for the dark Higgs boson in existing and projected proton beam-dump experiments. We show that future searches at experiments like Xenon1T or LDMX can probe all the relevant parameter space, complementing the various upcoming indirect constraints from astrophysical observations.

---

<sup>\*a</sup> [luc.darme@ncbj.gov.pl](mailto:luc.darme@ncbj.gov.pl)

<sup>†b</sup> [soumya.rao@ncbj.gov.pl](mailto:soumya.rao@ncbj.gov.pl)

<sup>‡c</sup> [leszek.roszkowski@ncbj.gov.pl](mailto:leszek.roszkowski@ncbj.gov.pl)

# Contents

<b>1</b>	<b>Introduction</b>	<b>2</b>
<b>2</b>	<b>Minimal dark sector models and bounds on the dark photon</b>	<b>4</b>
2.1	Lagrangian, masses and lifetimes . . . . .	4
2.2	Dark Higgs boson lifetime . . . . .	6
2.3	Constraints on the dark photon . . . . .	8
<b>3</b>	<b>Light DM phenomenology</b>	<b>9</b>
3.1	Relic density . . . . .	9
3.2	Direct and indirect detection bounds . . . . .	11
<b>4</b>	<b>Light dark Higgs boson</b>	<b>13</b>
4.1	Beam dump experiments . . . . .	13
4.2	BBN constraints . . . . .	19
<b>5</b>	<b>Summary and conclusions</b>	<b>22</b>
<b>A</b>	<b>Differential production rate of dark Higgs boson from meson decay</b>	<b>26</b>

## 1 Introduction

Among the many puzzles facing the Standard Model (SM) of particle physics, the issue of dark matter (DM) is certainly one of the most pressing. While the prime candidate of the last decades has been the Weakly Interactive Massive Particle (WIMP, see, e.g. [1, 2] for the latest reviews), direct, indirect and collider searches have so far failed to give an uncontroversial signal of such particles. Among the alternative ideas for dark matter that have emerged over the years, sub-GeV dark matter is gaining momentum, thanks both to a rich upcoming experimental program and to the fact that, similarly to the WIMP, it relies on the robust, UV-insensitive, thermal freeze-out mechanism to achieve the correct relic density (see [3] and [4] for reviews). These dark matter scenarios typically involve a dark matter candidate interacting with SM particles through a light mediator. In this article we shall focus on a specific class of models where the mediator is a new gauge boson,  $V$ , corresponding to a spontaneously broken new abelian gauge group  $U(1)_D$ , because of their viability in providing a light thermal dark matter as well as because of many experimental searches devoted to such models. We will refer to this new gauge boson as the *dark photon* in the following.

Since the new  $U(1)_D$  gauge group can mix with the Standard Model  $U(1)_Y$  gauge group, the dark photon acts as a proper mediator between the dark and visible sectors. Such dark gauge groups have been particularly often used in a dark matter context due to their interesting properties and experimental prospects for detection (some very recent examples are, e.g. [5, 6, 7, 8, 9, 10, 11, 12, 13]). For instance, they can give rise to simple Self-Interacting Dark Matter models (SIDM, see [14] for the latest review) which could lead to better agreement between numerical simulations and the astrophysical observations.

One of the simplest and experimentally-motivated way to generate the dark photon mass perturbatively is through a “dark Higgs mechanism”. This assumes the presence

of an additional dark Higgs boson which gives the dark photon its mass through a Vacuum Expectation Value (VEV)  $v_S$ . Thus, a complete, self-consistent “dark sector” contains a dark matter candidate, the dark photon and the dark Higgs boson. Crucially, both the dark Higgs boson mass and the dark photon mass are proportional to  $v_S$ , so that a light dark photon should typically be accompanied by a light dark Higgs boson.<sup>1</sup> Note that a popular alternative for  $U(1)$  extensions of the Standard Model consists in introducing a Stueckelberg field along with a mass term for the new gauge boson, see e.g. [16]. We focus instead in this paper on the phenomenologically-richer (in particular with respect to the pseudo-Dirac dark matter case) and experimentally well-grounded Higgs mechanism.

Paradoxically, most of the literature on the field either focused on the dark Higgs boson, with or without the dark photon, or assumed that it decouples from the rest of the spectrum and concentrated on the dark matter and the dark photon only (one of the recent exceptions is [17] with a focus on the relic density constraint). In contrast, we present in this paper two minimal, self-consistent and perturbative models for the dark sector and systematically study the large part of the parameter space where the dark Higgs boson is light. In this case the dark photon, dark matter and dark Higgs boson must all be considered simultaneously.

As we will see below, the most important characteristic of a light dark Higgs boson is the fact that its lifetime is typically of order of one second or longer. Indeed, when the dark Higgs boson is lighter than the dark photon and of twice the dark matter mass, its decay is particularly suppressed as it can only proceed through a loop-induced coupling to light Standard Model particles. Such long-lived dark Higgs boson have been studied independently for several years and have been shown to possibly leave a signal in long baseline neutrino experiments and more generally in so-called “beam-dump” experiments (see, e.g. [18, 19, 20, 21]). Light dark Higgs boson originating for instance from the decay of a light meson can travel through the shielding of these beam-dump experiments and subsequently decay in the downstream detector.<sup>2</sup> We will re-evaluate this particular search strategy for detecting dark Higgs bosons and show that they are currently not sensitive enough to reach the thermal value target in our two minimal models.

The second main result is that the relic density calculation is thoroughly modified by the presence of new dark matter annihilation channels involving a dark Higgs boson. In particular, the long lifetime of the dark Higgs boson implies that the thermal freeze-out mechanism proceeds as in a two-component dark matter scenario. However, its presence also opens up new additional  $s$ -wave annihilation channels for dark matter at the time of recombination and leads therefore to severe bounds from CMB observations [26, 27].

Finally, a long-lived dark Higgs boson is constrained by Big Bang Nucleosynthesis (BBN) related data [28, 29], especially given that its metastable density obtained from thermal freeze-out can be larger than that of the dark matter. Nonetheless, we will show

---

<sup>1</sup>The dark Higgs boson suffers from the same, and actually much larger naturalness problem as the Standard Model Higgs boson. We will assume that this problem is decoupled from our analysis (for instance that any supersymmetry-related fields are heavy enough to have a negligible influence). See in particular [15] for a discussion of a dark sector in a supersymmetric context.

<sup>2</sup>This is similar to the idea that beam-dump experiments can create a detectable “dark matter beam” when dark matter is light (typically below a few GeV) which has received more attention in recent years (see, e.g. [18, 22, 23, 24, 25]).

that light dark Higgs bosons in our two minimal dark sector models have metastable density substantially smaller than the Higgs portal case and can alleviate significantly the bounds presented in [28].

The paper is organized as follows. We first present in Sec. 2 two models of the dark sector framework, as well as existing constraints on the dark photon from various experiments. We then focus in Sec. 3 on the dark matter candidate and the effect of the presence of the dark Higgs boson on its relic density and on the constraints from CMB. Section 4 discusses detection prospect for the dark Higgs boson in beam-dump experiments as well as constraints related to BBN. Finally, in Sec. 5 we summarize our results and conclude. The appendix contains additional details on the calculation of dark Higgs boson production cross section from light mesons decay.

## 2 Minimal dark sector models and bounds on the dark photon

We present in this section two minimal, self-consistent dark sector models for a sub-GeV dark matter. As was discussed in the Introduction, such dark sectors typically include three types of fields:

- an extra gauge boson (called “dark photon” in the following)  $V$  corresponding to “dark” gauge group  $U(1)_D$  with a gauge constant  $g_V$ ;
- a complex scalar  $S$  with charge  $q_S$ , called henceforth “dark Higgs boson”. It spontaneously breaks the dark gauge group through a VEV,  $v_S$ ;
- a dark matter particle  $\chi$  with charge  $q_\chi$ . We will consider both a complex scalar and a Majorana fermion dark matter candidate. As usual, we will assume that a discrete  $\mathbb{Z}_2$  symmetry protects the dark matter from decaying.

### 2.1 Lagrangian, masses and lifetimes

The gauge and matter content that we are considering implies that the dark sector can be coupled to the SM either through kinetic mixing between the two abelian gauge groups or by mixing between the SM Higgs  $H$  and the dark Higgs boson  $S$ . While both portals are a priori open, in this article we will focus on the vector portal. We will furthermore argue below that this is the most natural choice given the sub-GeV mass domain we are interested in. The kinetic mixing can in principle arise from loops of heavy fields charged under both gauge groups. We will assume in the following that they are safely decoupled at the energy scale that we consider.

Given that the dark matter candidates must be charged under the new gauge group  $U(1)_D$ , care must be taken when choosing them such that the dark gauge group remains anomaly-free. In particular, this excludes one single Majorana dark matter candidate, albeit a non-minimal scenario with a second heavier Majorana field canceling the anomaly is still possible. Consequently, we will consider in this paper two minimal, self-consistent, models for the dark matter candidates:

- model  $pDF$ : the pseudo-Dirac fermion case, where a Dirac fermion  $\chi = (\chi_L, \chi_R^\dagger)$  dark matter acquires additional Majorana masses from its Yukawa interactions with the dark Higgs boson;

- model  $CS$ : the complex scalar dark matter case, where we also denote the dark matter field by  $\chi$ .

The simplest charge assignment in the  $pDF$  case is a  $U(1)_D$  charge  $+2$  for the dark Higgs boson  $S$  and  $\pm 1$  for the two dark matter fermions  $\chi_L$  and  $\chi_R$ . In the  $CS$  case, we assign a charge  $+1$  to the dark Higgs boson  $S$  and  $+1$  to the complex scalar dark matter  $\chi$ .

The effective Lagrangian for the dark photon vector and the dark Higgs boson fields in these two minimal dark sector models is then given by

$$\mathcal{L}_V = -\frac{1}{4}F'^{\mu\nu}F'_{\mu\nu} - \frac{1}{2}\frac{\varepsilon}{\cos\theta_w}B_{\mu\nu}F'^{\mu\nu}, \quad (2.1)$$

$$\mathcal{L}_S = (D^\mu S)^*(D_\mu S) + \mu_S^2|S|^2 - \frac{\lambda_S}{2}|S|^4 - \frac{\lambda_{SH}}{2}|S|^2|H|^2, \quad (2.2)$$

while the DM field is introduced either as a scalar or a fermion through the Lagrangian

$$\mathcal{L}_{pDF}^{\text{DM}} = \bar{\chi}(i\not{D} - m_\chi)\chi + V_{pDF}^m(S, \chi), \quad (2.3)$$

$$\mathcal{L}_{CS}^{\text{DM}} = (D^\mu\chi)^*(D_\mu\chi) - m_\chi|\chi|^2 + V_{CS}^m(S, \chi), \quad (2.4)$$

where  $V_{pDF}$  and  $V_{CS}$  describe the mixing of the DM particle with the dark Higgs boson  $S$ . We parametrize them as

$$V_{pDF} = y_{SL}S\chi_L\chi_L + y_{SR}S\chi_R^c\chi_R^c + \text{h.c.}, \quad (2.5)$$

$$V_{CS} = \lambda_\chi|\chi|^4 + \lambda_{\chi S}|\chi|^2|S|^2 + \lambda_{\chi H}|\chi|^2|H|^2. \quad (2.6)$$

If  $\mu_S^2 > 0$ , and in the relevant limit where  $\lambda_{SH} \ll \lambda_S, \lambda_H$ , we can solve the tadpole equations for the VEVs of the SM Higgs  $v_H$  and of the dark Higgs boson  $v_S$ , leading to

$$v_S^2 = \frac{1}{\lambda_S}\left(\mu_S^2 - \frac{\lambda_{SH}}{2\lambda_H}\mu_H^2\right), \quad (2.7)$$

$$v_H^2 \simeq \frac{\mu_H^2}{\lambda_H}$$

where  $\mu_H^2$  and  $\lambda_H$  are respectively the SM Higgs mass term and self quartic coupling. At zeroth order in  $v_S/v_H$ , the dark Higgs boson mass  $M_S$  and dark photon mass  $M_V$  are

$$M_S = \sqrt{2\lambda_S}v_S, \quad (2.8)$$

$$M_V = g_V q_S v_S = \left(\frac{q_S g_V}{\sqrt{2\lambda_S}}\right) M_S, \quad (2.9)$$

where we have introduced the dark Higgs boson  $U(1)_D$  charge  $q_S$ . In particular, the dark Higgs boson is lighter than the dark photon when

$$\sqrt{2\lambda_S} < q_S g_V.$$

This case will be of particular interest since the dark Higgs boson is then long-lived, as we will see in the next section.

Notice that for typical SM-like values  $\lambda \sim 0.1$  and  $g_V \sim 0.5$ , the dark Higgs boson is indeed lighter than the dark photon. Furthermore, when the dark gauge coupling is

chosen near its perturbativity bound with  $\alpha_D \equiv g_V^2/4\pi$  of order 0.5, then having a dark Higgs boson heavier than the dark photon leads to  $\lambda_S > 1.25q_S^2$  and therefore possible non-perturbative behavior in the dark sector. For large values of  $\alpha_D$ , assuming the dark Higgs boson to be heavy enough to completely decouple from the rest of the dark sector is hence impossible in a minimal perturbative setup.

The kinetic mixing parameter should be small enough to avoid various experimental bounds discussed in the following sections. In a Grand Unified Theory context, the required small values for  $\varepsilon$  could be obtained from loops of heavy particles charged under both the SM hypercharge  $U(1)_Y$  and the new  $U(1)_D$  gauge group [30], with values between  $10^{-2}$  and  $10^{-5}$  depending on whether the mixing is generated at one or two-loops.<sup>3</sup> Notice that after diagonalizing the gauge kinetic terms, dark sector particles remain neutral under electromagnetism, but Standard Model fields acquire an  $\varepsilon$ -suppressed coupling to the dark photon.

Finally, in the  $pDF$  case, the dark Higgs boson VEV leads to Majorana mass terms for the left-handed and right-handed components of  $\chi$ . After diagonalizing the mass matrix, the lightest eigenstate  $\chi_1$  becomes our dark matter candidate. Notice that in principle  $y_{SL} \neq y_{SR}$  so that gauge coupling of schematic form  $\chi_1\chi_1V$  and  $\chi_2\chi_2V$  are a priori generated (albeit typically suppressed compared to  $\chi_1\chi_2V$  term).

## 2.2 Dark Higgs boson lifetime

When the tree-level decay of dark Higgs boson to dark matter is kinematically forbidden and its mixing with SM Higgs boson is negligible, the only decay mode available is through a triangular diagram of the form given in Fig. 1a. Furthermore, when  $M_S < 2m_\mu$  the dominant decay mode is  $S \rightarrow e^+e^-$  with the dark Higgs boson width given by [32]

$$\Gamma_{S \rightarrow ee} = \frac{\alpha_D \alpha^2 \varepsilon^4 M_S}{2\pi^2} \frac{m_e^2}{M_V^2} \left(1 - 4 \frac{m_e^2}{M_S^2}\right)^{3/2} \left| I\left(\frac{M_S^2}{M_V^2}, \frac{m_e^2}{M_V^2}\right) \right|^2, \quad (2.10)$$

where the loop function is expressed as

$$I(x_s, x_e) = \int_0^1 dy \int_0^{1-y} dz \frac{2 - (y+z)}{(y+z) + (1-y-z)^2 x_e - yz x_s}.$$

The above expressions also apply to the decay to muons by just replacing  $m_e$  with  $m_\mu$ . In particular, in the limit  $m_e \ll M_S, M_V$ , we have

$$\Gamma_{S \rightarrow ee} \propto \frac{\varepsilon^4 m_e^2}{M_V} \left(\frac{M_S}{M_V}\right).$$

The corresponding lifetime  $\tau_S$  is presented in Fig. 1b as a function of  $M_S/M_V$ , from which one can recover the exact value for any set of parameters using the previous scaling relations.

As an order of magnitude estimate, we then have

$$\tau_S \propto 2 \cdot 10^{-3} \text{ s} \times \left(\frac{\alpha_{\text{em}}}{q_S^2 \alpha_D}\right) \left(\frac{10^{-3}}{\varepsilon}\right)^4 \left(\frac{100 \text{ MeV}}{M_S}\right) \left(\frac{M_V}{2m_f}\right)^2, \quad (2.11)$$

---

<sup>3</sup>For more details about the limit case of an almost decoupled dark sector with freeze-in realization of the correct relic density, see [31].

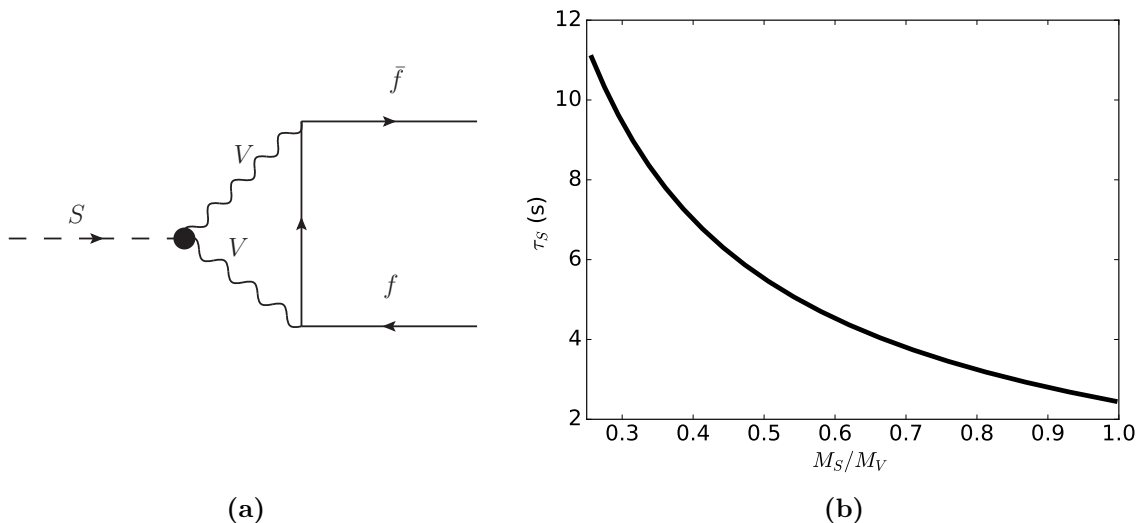


**Figure 1:** (a) Loop diagram for the dark Higgs boson decay with  $f$  denoting an SM fermion whose coupling to  $V$  is  $\varepsilon$ -suppressed. (b) Dark Higgs lifetime in seconds as a function of the ratio  $M_S/M_V$  for  $\alpha_D = \alpha_{\text{em}}$ ,  $\varepsilon = 0.001$  and  $M_V = 200$  MeV.

where  $f$  are the kinematically accessible SM fermions,  $\alpha_{\text{em}}$  is the electromagnetic fine-structure constant. In particular for  $M_S$  below the dimuon mass threshold we find

$$\tau_S \propto 10 \text{ s} \times \left( \frac{\alpha_{\text{em}}}{q_S^2 \alpha_D} \right) \left( \frac{10^{-3}}{\varepsilon} \right)^4 \left( \frac{50 \text{ MeV}}{M_S} \right) \left( \frac{M_V}{100 \text{ MeV}} \right)^2. \quad (2.12)$$

In principle, the mixing between the Standard Model Higgs and the dark Higgs boson through the mixing quartic coupling  $\lambda_{SH}$  could lead to additional decay channels. However, since the Higgs boson VEV contributes at tree level to the dark Higgs boson mass by  $\lambda_{SH} v^2$  we need

$$\lambda_{SH} \sim \frac{M_S^2}{v_H^2} \sim 10^{-8} - 10^{-6}, \quad (2.13)$$

for a dark Higgs boson mass between 10 and 100 MeV. If the dark Higgs boson could only decay to  $e^+e^-$  through its mixing with the SM Higgs, its lifetime  $\tau_{S,H\text{mix}}$  would then be parametrically given by

$$\tau_{S,H\text{mix}} \propto 1 \cdot 10^6 \text{ s} \times \left( \frac{100 \text{ MeV}}{M_S} \right) \left( \frac{100 \text{ MeV}}{M_V} \right)^2 \left( \frac{10^{-6}}{\lambda_{SH}} \right)^2 \left( \frac{q_S^2 \alpha_D}{\alpha_{\text{em}}} \right). \quad (2.14)$$

This implies that, unless one is prepared to significantly tune the theory to ensure a light dark sector while keeping a large  $\lambda_{SH}$ , the decay through SM Higgs mixing should be significantly smaller than the loop-induced one.

In the rest of this article, we will therefore neglect the Higgs-portal related effects (which includes the quartic  $\lambda_{SH}$ , but also for simplicity, the dark matter/Higgs quartic  $\lambda_{\chi H}$  in the  $CS$  case).

Parameter	Description	Range	Prior
$\lambda_S$	Dark Higgs boson quartic coupling	$10^{-4}, 0.25$	Log
$g_V$	Dark gauge coupling	$5 \cdot 10^{-3}, 1.25$	Linear
$M_V$	Dark photon mass	10, 500	Log
$\varepsilon$	Kinetic mixing parameter	$1.5 \cdot 10^{-5}, 1.5 \cdot 10^{-3}$	Log
$m_\chi$	Complex scalar DM mass	10, 500 ( <i>CS</i> )	Log
	Dirac DM mass	10, 500 ( <i>pDF</i> )	Log
$\lambda_{S\chi}$	Quartic mixing between the dark Higgs boson and DM	$10^{-3}, 0.2$ ( <i>CS</i> )	Log
$\lambda_\chi$	Self DM quartic coupling	$5 \cdot 10^{-4}, 0.1$ ( <i>CS</i> )	Log
$y_{SL}$	Left-handed DM-dark Higgs boson Yukawa coupling	$10^{-3}, 0.7$ ( <i>pDF</i> )	Log
$y_{SR}$	Right-handed DM-dark Higgs boson Yukawa coupling	$10^{-3}, 0.7$ ( <i>pDF</i> )	Log

**Table 1:** Parameters of the models analyzed in this work. All parameters are initialized at the electroweak scale. Dimensionful quantities are given in MeV and  $\text{MeV}^2$ .

### 2.3 Constraints on the dark photon

If the dark matter is heavier than half of the dark photon mass, the dark photon decays mainly into a pair of leptons. This minimal scenario is mostly constrained by searches for bumps in the dilepton invariant spectrum at NA-48/2 [33], BaBar [34] and LHCb [35], setting bounds for  $\varepsilon \lesssim 10^{-3}$ . Slightly less competitive bounds also arise from rare meson decays. For very small kinetic couplings leading to a long-lived dark photon decaying to visible sector, one can also obtain bounds from electron beam-dump experiments like E137, E141 or E774. These searches hence give a lower bound on the kinetic mixing for a dark photon with mass in the tens of MeV range (see, e.g. [4] for a summary of the current bounds).

The most relevant case for the parameter space considered here is when the dark photon decay channel to dark matter is kinematically open, so that one should search for the missing momentum carried away by the Dark matter particles [36, 37]. The strongest bounds are currently set by searches at BaBar [38] and NA64 [39]. More precisely, the BaBar analysis searches for narrow peaks in the distribution of missing mass arising from  $e^+e^- \rightarrow \gamma V$  events. Their limit excludes the region  $\varepsilon > 10^{-3}$  for the dark photon mass range we consider, which in particular rules out the dark photon explanation for the  $(g-2)_\mu$  excess. Secondly, the NA64 Collaboration recently released bounds on the decay  $V \rightarrow \text{invisible}$ . Their limits significantly exceed the one set by BaBar for  $M_V \lesssim 100$  MeV, reaching  $\varepsilon < 10^{-4}$  below 10 MeV. An explicit visualization of these bounds will be shown below in Fig. 3 in Sec. 3.2. Note that the projected bounds from the LDMX proposal (see, e.g. [3]) will cover almost all of the parameter space consistent with the relic density thermal value target as shown in Fig. 3.



In the following and for all the numerical results, we used the code `MultiNest` [40] to direct the scanning procedure, based on the dark matter relic density. All data points presented in this paper are therefore compatible with the result from the Planck Collaboration [41]  $\Omega h^2 = 0.1188 \pm 0.0010$  at 95% CL. The interfaces with the various public codes used here is done with the help of the private code `BayesFITS`. We use a slightly modified version of `MicrOMEGAs` v.4.3.5 [42] (and of its two-component dark matter module). We evaluate the spectrum from the non-SUSY `SPheno` [43, 44] code generated by `SARAH` (see Refs. [45, 46, 47]). We use renormalization group evolution of the hidden sector parameters to ensure their perturbativity up to the electroweak scale, and evaluate all masses at tree-level due to the light scale considered. Finally, the estimation of the number of events in beam-dump experiments is obtained from a substantially modified version of `BdNMC` from [24] (more particularly, we have used the original code to extract the distributions of initial mesons and expanded its routines to the production and detection processes relevant for the dark Higgs boson).

In the following, we will restrict our analysis to the case where the dark Higgs boson is below the dimuon threshold, so that it can only decay to an  $e^+e^-$  pair. The dark photon is also considered to be lighter than around 500 MeV, so that the leptonic decay channels still dominate its decay width compared to hadronic ones (see [48]). We summarize the independent parameters and their scanned ranges and priors in Table 1. Note that we do not vary the SM Higgs parameters. In particular, we take advantage of the relation (2.8) to trade  $v_S$  for  $M_V$  as an input parameter, so that we vary  $g_V, \varepsilon, M_S, M_V, m_\chi, y_{SL}$  and  $y_{SR}$  in the *pDF* model and  $g_V, \varepsilon, M_S, M_V, m_\chi, \lambda_{S\chi}$  and  $\lambda_\chi$  in the *CS* model.

### 3 Light DM phenomenology

In this section we discuss the phenomenology of the light DM candidate in our two minimal dark sector models. We focus particularly on the relic density constraints and on the bounds from CMB power spectrum for *s*-wave annihilation processes occurring during the recombination era. We begin with a discussion of relic density for the pseudo-Dirac fermion (*pDF* case) and complex scalar (*CS* case) DM candidates. In the following, the dark matter mass is denoted by  $M_\chi$ , which hence refers to the mass of lightest mass eigenstate  $\chi_1$  in the *pDF* case.

#### 3.1 Relic density

The relic density of DM in the standard freeze-out scenario is obtained by solving the following Boltzmann equation

$$\frac{dn_\chi}{dt} + 3Hn_\chi = -\langle\sigma v\rangle (n_\chi^2 - (n_\chi^{\text{eq}})^2) , \quad (3.1)$$

where  $n_\chi$  is the density of the DM species and  $\langle\sigma v\rangle$  is the thermally averaged annihilation rate of DM. The thermally averaged annihilation rate is given by [49]

$$\langle\sigma v\rangle = \frac{1}{8M_\chi^4 T K_2(M_\chi/T)} \int_{4M_\chi^2}^{\infty} \sigma \sqrt{s} (s - 4M_\chi^2) K_1(\sqrt{s}/T) ds , \quad (3.2)$$

where  $K_1$  and  $K_2$  are modified Bessel's functions. A useful parametrization of the annihilation rate is in terms of *s*-wave and *p*-wave annihilations like  $\langle\sigma v\rangle \equiv \sigma_0 x^{-n}$ ,

with  $x = m_\chi/T$ . Here  $n = 0$  for  $s$ -wave and  $n = 1$  for  $p$ -wave annihilation. In this parametrization,  $x$  at freeze-out is given by [50]

$$x_f = \ln \left( 0.038(n+1) \frac{g}{\sqrt{g_*}} M_{Pl} M_\chi \sigma_0 \right) - \left( n + \frac{1}{2} \right) \ln \left[ \ln \left( 0.038(n+1) \frac{g}{\sqrt{g_*}} M_{Pl} M_\chi \sigma_0 \right) \right], \quad (3.3)$$

where, following the notation of [50], we note that  $g$  represents the DM degrees of freedom, while  $g_*$  and  $g_{*,s}$  represent the number of relativistic degrees of freedom at freeze-out. With the above expression for  $x_f$  one can write the approximate expression for relic density as

$$\Omega h^2 = 0.1 \left( \frac{(n+1)x_f^{n+1}}{(g_{*,s}/g_*^{1/2})} \right) \frac{10^{-26} \text{ cm}^3/\text{s}}{\sigma_0}. \quad (3.4)$$

In the two minimal dark sector scenarios we consider, the dark matter particle can be either a pseudo-Dirac fermion ( $pDF$  case) or a complex scalar ( $CS$  case). In both cases, including the dark Higgs boson field leads to several new annihilation channels in a similar manner to the usual supersymmetric WIMP. The usual behavior considered by the previous literature corresponds to the case when the dark Higgs boson is significantly heavier than the dark matter candidate so that annihilation into dark Higgs boson is suppressed even with thermal effects included. The dominant process is a  $s$ -channel annihilation to SM particles through an off-shell dark photon with the annihilation cross-section, for instance in the  $CS$  case given by [51, 52]

$$\sigma_0 = 2.8 \cdot 10^{-25} \text{ cm}^3/\text{s} \times \left( \frac{\varepsilon}{10^{-3}} \right)^2 \left( \frac{\alpha_D}{\alpha_{em}} \right) \left( \frac{M_\chi}{100 \text{ MeV}} \right)^2 \left( \frac{100 \text{ MeV}}{M_V} \right)^4. \quad (3.5)$$

Using the above expression for  $\sigma_0$  in Eq. (3.3) and Eq. (3.4) we arrive at the following estimate for the relic density

$$\Omega h^2 \sim 0.1 \times \left( \frac{10^{-3}}{\varepsilon} \right)^2 \left( \frac{0.1}{\alpha_D} \right) \left( \frac{25 \text{ MeV}}{M_\chi} \right)^2 \left( \frac{M_V}{75 \text{ MeV}} \right)^4. \quad (3.6)$$

On the other hand, for  $M_\chi \sim M_S$ , dark matter annihilation into final states involving dark Higgs boson become relevant. They proceed either through a  $t$ -channel exchange of a dark matter particle, or through a dark Higgs boson  $s$ -channel. These new mechanisms alone could explain the current relic density for a dark sector coupling between dark Higgs boson and dark matter in the range we consider, and therefore have to be taken into account. A key complication of this setup is that the dark Higgs boson is a metastable particle with lifetime above 0.01 s in almost all of our parameter space. Consequently, thermal freeze-out proceeds akin to a two-component dark matter scenario. This is especially relevant when the mass of the dark matter and of the dark Higgs boson are of the same order, so that both  $\chi\chi \rightarrow SS$  and  $SS \rightarrow \chi\chi$  processes are occurring at the time of dark matter freeze-out. This annihilation channel is similar to the “secluded” regime in classic Higgs-portal scenarios [53, 54, 55] although the metastability of the dark Higgs boson implies in our case that the reverse processes  $SS \rightarrow \chi\chi$  must be included compared to these references. Furthermore, in the case

of the  $pDF$  model, the fact that we consider the Yukawa couplings to the two Weyl components to be different in general (i.e,  $y_{SL} \neq y_{SR}$  in contrast with [56]) implies that the annihilation channels  $\chi_1\chi_1 \rightarrow e^+e^-$  and  $\chi_1\chi_2 \rightarrow SS$  are also available.

In Fig. 2 we represent the relevant annihilation channels that contribute to the relic density in the  $CS$  case and the  $pDF$  case. We see from the figure that in the  $CS$  case, when  $M_S \lesssim M_\chi$  the  $SS$  channel dominates (this region is excluded by CMB bounds) and when  $M_S \gtrsim M_\chi$  there are no  $S$  final states with only the  $e^+e^-$  channel remaining available to achieve the correct relic density. For the  $pDF$  case the picture is more complicated due to the presence of coannihilation channels.<sup>4</sup> However, one still sees the  $e^+e^-$  channel being predominant in the  $M_S > M_\chi$  region, and the  $SS$  channel dominating when  $M_\chi \simeq M_S$ . In the very low mass region ( $M_\chi < 10$  MeV), our choice of parameter range (and in particular  $m_\chi > 10$  MeV) implies that most of our points have a very large splitting between both dark matter components  $\chi_1$  and  $\chi_2$ .<sup>5</sup> In particular, the channel  $\chi_1\chi_1 \rightarrow e^+e^-$  then becomes the dominant annihilation channel. Finally, the presence of the “reverse”  $SS \rightarrow \chi\chi$  channel implies that for some of our points in which the  $\chi\chi \rightarrow SS$  annihilation process dominates, the thermal value target is in fact achieved by the subdominant channel  $e^+e^-$ , while for some points in the  $M_\chi > M_S$  region the choice of couplings  $y_{SL}$ ,  $y_{SR}$  and  $\alpha_D$ , leads to  $e^+e^-$  being the dominant channel.

Thus the presence of dark Higgs bosons changes significantly the relic density evaluation in our two models. However, it also leads to two additional difficulties. First, the presence of a large metastable density of dark Higgs boson after thermal freeze-out may lead to strong tensions with BBN. We will explore this aspect in Sec. 4.2. Second, as we will see in the next section, the presence of the new annihilation channels, while significantly reducing the constraints arising from the relic density, may on the other hand be in strong tension with indirect bounds from CMB power spectrum.

### 3.2 Direct and indirect detection bounds

The CMB power spectrum has been measured with high precision and as such can impose stringent constraints on the nature of DM. In particular DM that injects energy in the form of electromagnetically interacting SM particles in the inter-galactic medium (IGM) can significantly alter the recombination history of the universe by ionizing and heating the IGM gas. Such injections from DM annihilation can be parametrized as  $p_{ann} = f\langle\sigma v\rangle/M_\chi$ , where  $f$  denotes the efficiency with which the energy injected by DM annihilations is transferred to the IGM. Usually the constraints from  $s$ -wave DM annihilations which do not depend on velocity of DM can be very stringent and virtually rule out most models with  $m_\chi < 10$  GeV [26]. Since electrons and photons are the most efficient at ionizing the IGM, the annihilation channels that are most severely constrained produce  $e^-$ s and  $\gamma$ -rays in their final states.

For the  $pDF$  model, when  $\lambda_{S\chi_L} \neq \lambda_{S\chi_R}$  annihilation into an  $e^+e^-$  pair as  $\chi_1\chi_1 \rightarrow V^* \rightarrow e^+e^-$  becomes accessible. It is however safely suppressed by mixing matrices elements and the off-shell nature of the  $V$  in all our parameter space.

---

<sup>4</sup> We have estimated the dominant annihilation cross-sections by summing the contributions from both annihilation and co-annihilation channels.

<sup>5</sup>The mass matrix for dark matter in this case has a seesaw structure, which leads to the large splitting. There is no such mechanism for the  $CS$  case.

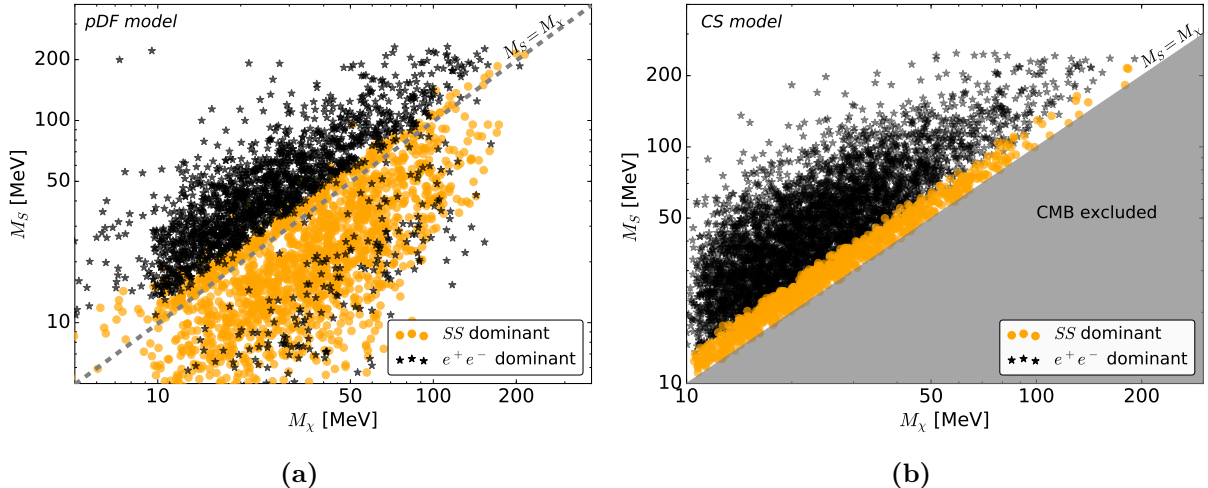


**Figure 2:** Points satisfying the dark matter relic density constraints in the  $M_\chi - M_S$  plane, sorted according to the dominant annihilation channels at freeze-out in the  $pDF$  case (a) and the  $CS$  case (b). In (b), the region with  $M_\chi > M_S$ , which is excluded by CMB bounds, has been indicated.

The situation is very different in the  $CS$  model, as  $t$ -channel annihilation into dark Higgs boson  $\chi\chi \rightarrow SS$  is completely unsuppressed when  $M_S < M_\chi$ . Hence CMB bounds essentially rule out this portion of the parameter space. Notice that in both cases, if  $M_\chi > M_V$ , other annihilation channels involving the dark photon open up which could lead to more severe bounds. However, they typically also significantly reduce the relic density, limiting the possibility to reach the thermal value target for the range of  $\varepsilon$  we consider in this paper.

The bounds from CMB depend in principle on the annihilation products (in particular they have been calculated for the  $e^+e^-$ , and  $e^+e^-$  via  $S$  decays). However, they do not differ significantly in the dark matter mass region we are interested in. In the very low dark matter mass region of our plot ( $M_\chi \lesssim 10$  MeV), BBN-related bounds from energy injection from dark matter annihilation at freeze-out could become relevant [57]. However, they are model dependent and may in particular be modified due to the presence of a potentially long-lived dark Higgs.

Finally, in the case of complex scalar dark matter  $CS$ , direct detection experiments searching for DM scattering through electron recoil are also relevant for sub-GeV dark matter. Different target materials such as noble liquids, semiconductors, scintillators and superconductors have been proposed for such searches (see [3, 4] for a discussion of these searches). In the case of noble liquid targets, searches for annual modulation signals through electron recoil were performed at XENON10 and XENON100 [60, 59], leading to the following bounds [61]

$$\begin{aligned} \sigma_{\text{Xe}}^{\text{SI}} &\simeq 4 \cdot 10^{-39} \text{cm}^2 \times \left(\frac{\varepsilon}{10^{-3}}\right)^2 \left(\frac{\alpha_D}{0.01}\right) \left(\frac{100 \text{ MeV}}{M_V}\right)^4 \\ &\lesssim \mathcal{L}(M_\chi) \cdot 10^{-38} \text{cm}^2, \end{aligned} \quad (3.7)$$

where the last inequality is the derived XENON10/XENON100 bound  $\mathcal{L}(M_\chi)$  which depends on the precise dark matter mass (see [59]). In addition, experiments based on

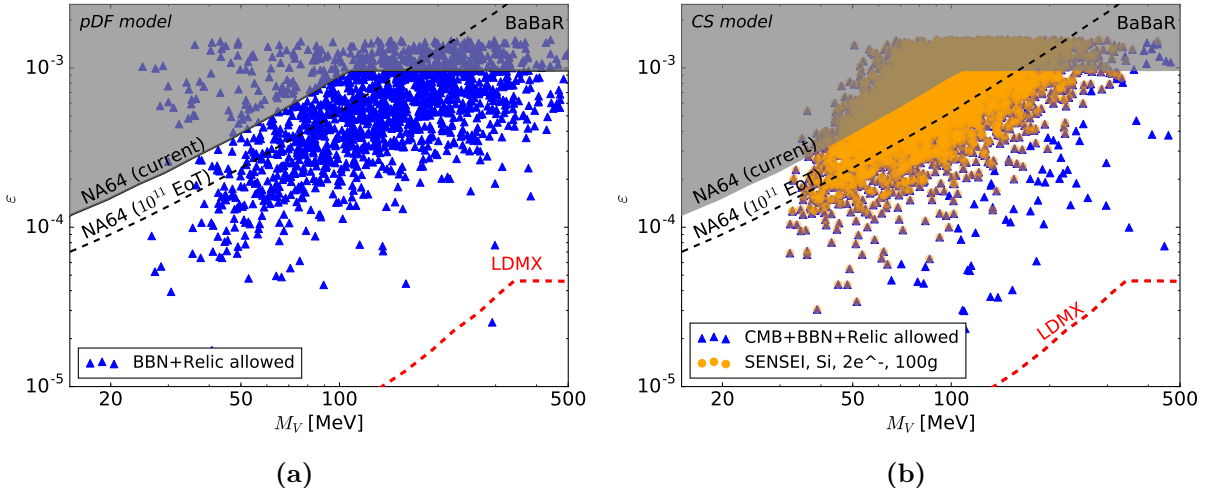


**Figure 3:** Constraints on the dark photon mass  $M_V$  and on the kinetic mixing parameter  $\epsilon$  from NA64 and BaBaR missing energy searches, with the projected bounds on a short time scale of SENSEI [58, 3] with one year exposure of a 100g detector (bounds from one year exposure of the annual modulation signals at Xenon1T according to [59] are essentially similar) and from the full dataset of NA64 (corresponding to  $10^{11}$  electrons on target, see [3]). Points satisfying the dark matter relic density and relevant BBN and CMB constraints are shown for the  $pDF$  model (a) and for the  $CS$  case (b). The dashed red line represents the projected LDMX bound [3].

semiconductors using silicon CCDs like SENSEI [58, 3] can also improve upon these bounds. We present in Fig. 3 the corresponding bound from SENSEI as function of the dark matter mass for all points of our scans satisfying the relic density constraint. The projected bound from SENSEI can probe almost all of the parameter space where we found the correct relic density (they are furthermore almost similar to one expected from annual modulation signals at XENON1T [59]). In future experiments using superconducting detectors based on aluminium can also probe this region of parameter space, but are perhaps more suited for sub-MeV range of masses. Finally, the rest of the parameter space will be totally covered by medium-term experiments, such as DAMIC-1K [3].

## 4 Light dark Higgs boson

We now turn to the second light state of our dark sector: the dark Higgs boson. As we have shown in Sec. 2.2, this particle is long-lived in most of our parameter space. We explore in this section two consequences of this long lifetime: the detection prospects at proton beam-dump experiments, and the constraints from BBN-related observables.

### 4.1 Beam dump experiments

Fixed target experiments are well suited for the detection of light dark sector particles. They typically involve a high-intensity, but relatively low-energy proton or electron

Name	Energy	Target Material	Distance	Length	Area
LSND	0.798 GeV	Water/high-Z metal	34 m	8.3 m	25.5 m <sup>2</sup>
MiniBooNE	8.89 GeV	CH <sub>2</sub>	490 m	Sphere	$R = 2.6$ m
SBND	8.89 GeV	CH <sub>2</sub>	112 m	5 m	16 m <sup>2</sup>

**Table 2:** Summary of the relevant characteristics of the experiments considered. Detector distances are taken from the beam target to the center of the detector. LSND has a cylindrical geometry, MiniBooNE a spherical one and SBND should have a square intersection with the beam axis.

Experiment	$\pi^0$ Distribution	$N_{\pi^0}$	$N_{\eta}/N_{\pi^0}$	$N_{\rho}/N_{\pi^0}$	$N_{\omega}/N_{\pi^0}$
LSND	Burman-Smith	$10^{22}$	/	/	/
MiniBooNE	Sanford-Wang	$2 \cdot 10^{20}$	0.33	0.05	0.046
SBND	Sanford-Wang	$6.6 \cdot 10^{20}$	0.33	0.05	0.046

**Table 3:** Summary of the relevant characteristics of mesons productions in the experiments considered. Note that the lower energy at LSND prevents the production heavier mesons.

beam impacting the target, producing a shower of secondary particles, which are later disposed off in a large shielding. Long-lived or stable dark matter particles are produced at a low rate in the target, but since they interact very weakly with the shielding, they travel to a downstream detector which can subsequently detect them.

In particular, when the dark photon decays into dark matter particles, it effectively produces a “dark matter beam” and the possible scattering of dark matter in the detector can then be estimated [18, 22, 23, 24, 25]. In particular, a case comparable to our fermion dark matter scenario  $pDF$  has been studied in [56].

In this section, we will focus instead on examining the dark Higgs boson detection prospects in three proton beam-dump experiments: LSND [62], miniBooNE [63] and the proposed SBND experiment at Fermilab [64]. The details of the experimental setups are presented in Table 2. These three experiments rely on proton beams with relatively low energy so that we expect dark sector production through bremsstrahlung and direct production to be sub-dominant compared to the meson decay mechanism [24].

Notice that past electron beam-dump experiments, like E137 [65], can also lead to dark sector beams through dark photon production by bremsstrahlung. However, the bounds on the kinetic mixing parameter  $\varepsilon$  derived from dark Higgs boson production and decay at these facilities were found in [15] (in a context roughly similar to ours – albeit in a supersymmetric model) to be always significantly weaker than the current missing energy bound  $\varepsilon < 10^{-3}$ . The case studied in [56], which we will consider in more details at the end of this section, is a notable exception.

#### 4.1.1 Dark Higgs boson production through meson decay

Proton beam-dump experiments could be practically seen as light meson factories, with around one neutral pion created for each proton on the target. We furthermore

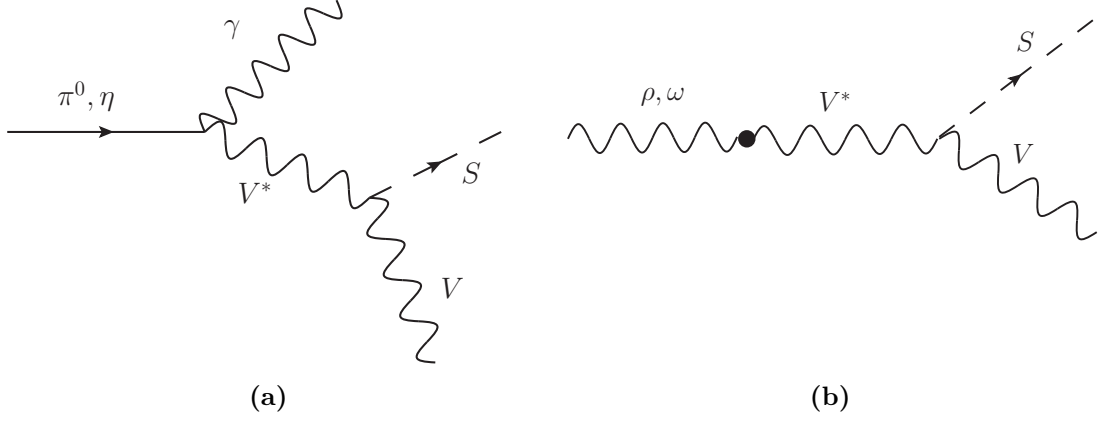


**Figure 4:** Dark Higgs production in scalar (a) and vector (b) meson decay through dark Higgstrahlung.

include the production of heavier  $\eta$ ,  $\rho$  and  $\omega$  mesons. The relevant number of mesons produced in each experiment is given in Table 3 based on [52, 66]. We simulate their kinematic distribution by using a weighted Burman-Smith distribution to account for the different target material used by the LSND experiment over its lifetime (water, then high-Z metal) and an averaged  $\pi^+$  and  $\pi^-$  Sanford-Wang distribution for MiniBooNE and SBND.

The produced meson has a tiny chance of decaying into dark sector particles. In this decay, dark Higgs boson can be produced from an excited dark photon through a “dark” Higgstrahlung mechanism. The processes for the scalar meson decay are

$$\pi^0, \eta \rightarrow \gamma V^*, V^* \rightarrow SV,$$

and for the vector meson case

$$\rho, \omega \rightarrow V^*, V^* \rightarrow SV.$$

The corresponding Feynman diagrams are shown in Fig. 4.

Focusing on the first process, we can write the branching ratio for a neutral pion as

$$\text{BR}_{\pi^0 \rightarrow \gamma SV} = \frac{1}{2m_{\pi^0}\Gamma_{\pi^0}} \int \frac{ds}{2\pi} d\Pi_{\pi^0 \rightarrow \gamma V^*} d\Pi_{V^* \rightarrow VS} |\mathcal{M}|^2, \quad (4.1)$$

where  $d\Pi_{\pi^0 \rightarrow \gamma V^*}$  and  $d\Pi_{V^* \rightarrow VS}$  represent the usual two-body decay phase space,  $|\mathcal{M}|^2$  is the squared, averaged amplitude,  $s$  is the squared momentum of the excited dark photon and is integrated between  $(M_V + M_S)^2$  and  $m_{\pi^0}^2$ . The relevant quantity for our Monte-Carlo simulation is the differential decay rate  $\frac{d\text{BR}_{\pi^0 \rightarrow \gamma SV}}{dsd\theta}$ , where  $\theta$  is the angle between the dark Higgs boson and the excited dark photon in the rest frame of the latter. We find (see Appendix A for details)

$$\frac{d^2\text{BR}_{\pi^0 \rightarrow \gamma SV}}{dsd\theta} = \text{BR}_{\pi^0 \rightarrow \gamma\gamma} \times \frac{\varepsilon^2 \alpha_D q_S^2}{8\pi} s \left(1 - \frac{s}{m_{\pi^0}^2}\right)^6 \times \frac{\sqrt{\lambda} (8M_V^2/s + \lambda \sin^2 \theta)}{(s - M_V^2)^2 + M_V^2 \Gamma_V^2} \sin \theta, \quad (4.2)$$



where  $q_S$  is the dark Higgs boson  $U(1)_D$  charge,  $\Gamma_V$  is the width of the dark photon (which can be neglected in practice) and  $\lambda$  is given by

$$\lambda \equiv \left(1 - \frac{(M_V + M_S)^2}{s}\right) \left(1 - \frac{(M_V - M_S)^2}{s}\right).$$

The case of the  $\eta$  meson is completely similar, with the replacement  $m_{\pi^0} \rightarrow m_\eta$  and  $\text{BR}_{\pi^0 \rightarrow \gamma\gamma} \rightarrow \text{BR}_{\eta \rightarrow \gamma\gamma} = 0.394$ . We have also checked agreement with the integrated standard results of [18].

The second process, corresponding to vector meson decays, is a simpler two-body decay. The branching ratio is given by

$$\text{BR}_{\rho \rightarrow SV} = \text{BR}_{\rho \rightarrow e^+e^-} \frac{\varepsilon^2 \alpha_D q_S^2}{\alpha_{em}} m_\rho^4 \frac{\sqrt{\lambda'} (12M_V^2/m_\rho^2 + \lambda')}{(m_\rho^2 - M_V^2)^2 + M_V^2 \Gamma_V^2}, \quad (4.3)$$

where

$$\lambda' \equiv \left(1 - \frac{(M_V + M_S)^2}{m_\rho^2}\right) \left(1 - \frac{(M_V - M_S)^2}{m_\rho^2}\right),$$

and similarly for  $\omega$  mesons.

While the processes described above are typically suppressed compared to the on-shell production of dark matter particles from dark photon decay, the dark Higgs boson on the other hand is easier to detect as one can search directly for its decay products. Note that due to the absence of gauge vertices between two dark Higgs bosons and the dark photon, the only scattering process available is through dark Higgs boson mixing with the SM Higgs boson and is therefore negligible here.

#### 4.1.2 Dark Higgs boson decay and detection

As discussed before, when the decay of a dark Higgs boson into two dark photons or dark matter particles is kinematically forbidden, it is long-lived and can only decay to an  $e^+e^-$  pair through the loop-diagram process shown in Fig. 1a. This is in principle a very distinctive signature compared to dark matter scattering. In practice however, most of the existing experimental bounds are derived from neutrino-electron scattering signal, which consist of only one charged track. In detail, for each of the considered experiments, we have:

- LSND: We choose to use the search [67] for electron neutrino  $\nu_e$  via the inclusive charged-current reaction  $\nu_e + C \rightarrow e^- + X$ .<sup>6</sup> Following [21], we will consider that the outgoing  $e^+e^-$  pair is interpreted as a single electron event satisfying the energy cut,  $60 \text{ MeV} < E_{e^+} + E_{e^-} < 200 \text{ MeV}$  and use the electron detection efficiency of around 10%. Given the uncertainties presented in [67] (see especially Fig 29 and the Tables IV and V), and the fact that the energy distribution of our process would not have been uniform, we will consider that 25 events should have been observed and draw our contours accordingly. As was already pointed out in [21] for dark photon searches, a re-analysis of the LSND data focused on pair of  $e^+e^-$  events and increasing the energy threshold would significantly improve the limit from this experiment.

---

<sup>6</sup>Note that this is not the search [68] which focused on the lower energy region  $18 \text{ MeV} < E_{e^+} + E_{e^-} < 50 \text{ MeV}$  used, e.g. in [56]. The cut on the electron energy made it unsuitable for our setup.



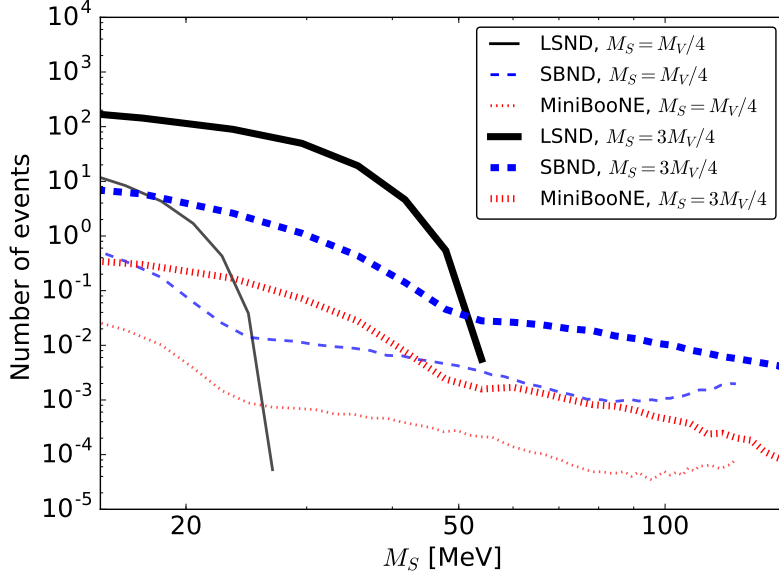


**Figure 5:** Number of events expected at LSND, miniBooNE and SBND experiments as a function of dark Higgs boson mass  $M_S$ . We show two mass ratios:  $M_S = M_V/4$  (thin lines) and  $M_S = 3/4M_V$  (thick lines). We have chosen the couplings to be  $\varepsilon = 0.001$  and  $\alpha_D = \alpha_{\text{em}}$ .

- MiniBooNE: We concentrate on the “off-target” dataset used in [69] for dark matter searches, and therefore require the electron and positron tracks to satisfy  $\cos \alpha > 0.99$  where  $\alpha$  is the angle to the beam axis and have energy in  $50 \text{ MeV} < E_{e^\pm} < 600 \text{ MeV}$ . The efficiency for detecting leptons is taken to be 35% from [70]. Following [56], we will require that both leptons are sufficiently separated so that miniBooNE could resolve both tracks (with a angular resolution of  $2^\circ$ ). Since no such search has been yet released, we can only give projections.
- SNBD: We will conservatively apply the same lepton detection efficiency and cut  $\cos \alpha > 0.99$  as in the MiniBooNE analysis for this experiment, as this is enough to significantly extend the reach of MiniBooNE.

Once the dark Higgs bosons have been produced, they will travel through the shielding before decaying into the detector. The probability of a decay event happening within the detector is simply given by

$$\mathcal{P}_d = \exp\left(-\frac{L_d}{\gamma v \tau_S}\right) \left[1 - \exp\left(-\frac{L_{\text{cr}}}{\gamma v \tau_S}\right)\right], \quad (4.4)$$

where  $\gamma$  is the Lorentz factor,  $L_d$  is the distance between the target and the entry point of the dark Higgs in the detector and  $L_{\text{cr}}$  is the length of the intersection of the dark Higgs trajectory with the detector. In the limit where  $\gamma v \tau_S \ll L_d, L_{\text{cr}}$  the probability reduces to

$$\mathcal{P}_d \simeq \frac{L_{\text{cr}}}{\gamma v \tau_S}.$$

The number of dark Higgs bosons detected scales as  $\varepsilon^6 \alpha_D^2$  so that even a tiny modification of the kinetic mixing will lead to drastic changes in the detection signature.

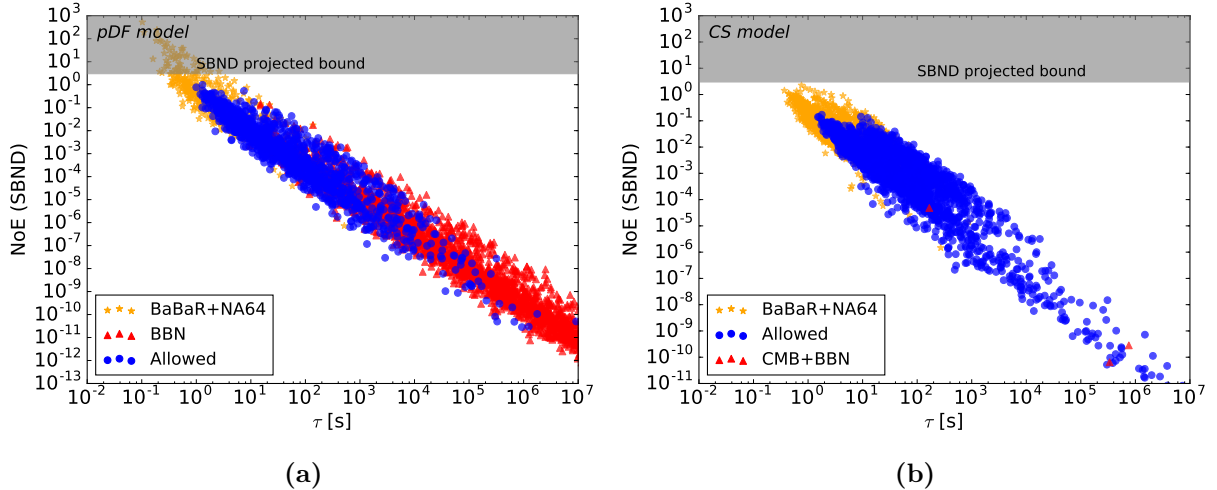


**Figure 6:** Number of events expected at the SBND experiment for all points satisfying the relic density bound as a function of the dark Higgs boson lifetime  $\tau_S$ . We show as orange stars all the points excluded by the missing energy searches, and as red triangles points excluded by relevant CMB and BBN observables. We show the reach of SBND assuming no event observed in the zero background hypothesis for the  $pDF$  case (a) and the  $CS$  case (b). The exclusion line is therefore drawn for 95% CL assuming a Poisson distribution (3 events).

We show in Fig. 5 the number of events expected in all three experiments considered here as a function of  $M_S$  in our  $pDF$  model. We have chosen  $\varepsilon = 0.001$  and  $\alpha_D = \alpha_{em}$  but the expected number of events for any other values of these parameters can be recovered from the previously mentioned scaling relations. In particular, notice that SBND will improve on the miniBooNE bound by one order of magnitude, provided a suitable search strategy is implemented.

Compared with the standard bounds from dark matter searches in this experiment, as in, e.g. [69, 24, 56], our expected number of events is even more sensitive to the kinetic mixing parameter  $\varepsilon$ . In both of our models, we found that the thermal value target is still out of reach of beam dump experiment as shown in Fig. 6, where we have shown the projected number of events at SBND. The cases of LSND and miniBooNE are similar, with no points compatible with the relic density constraint leading to more than a few expected events. Hence the situation for dark Higgs boson search at proton beam-dump experiments is relatively similar to the one for the dark matter scattering searches in the same detectors, with the thermal value target out of reach of current experiments [24]. One interesting exception in the  $pDF$  case was pointed out in [56]. When dark matter is produced from dark photon decay, the heaviest mass eigenstate  $\chi_2$  can only decay to  $\chi_1$  through an off-shell dark photon, in the process  $\chi_2 \rightarrow \chi_1 e^+ e^-$ , which leads to a long lifetime of order

$$\tau_{\chi_2} \sim 3 \cdot 10^3 \text{ m} \times \left( \frac{\alpha_{em}}{\alpha_D} \right) \left( \frac{0.1}{\Delta} \right)^5 \left( \frac{10^{-3}}{\varepsilon} \right)^2 \left( \frac{75 \text{ MeV}}{m_{\chi_1}} \right)^5 \left( \frac{M_V}{200 \text{ MeV}} \right)^4, \quad (4.5)$$

where we have introduced the splitting parameter between the two dark matter eigenstate  $\Delta = (M_{\chi_2} - M_{\chi_1})/M_{\chi_1}$ . While this is not long-lived enough to imply sizable

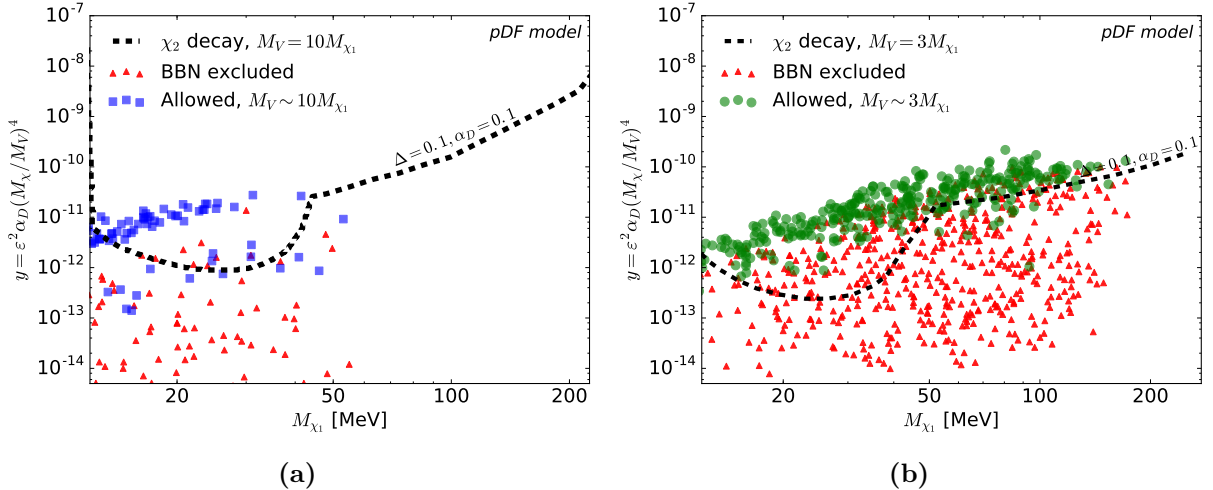


**Figure 7:** An example of bounds on the parameter  $y \equiv \varepsilon^2 \alpha_D (M_\chi/M_V)^4$  as a function of the DM mass  $M_\chi$  for  $\Delta \sim 0.1, \alpha_D \sim 0.1$  from [56]. We show the points from our scans satisfying all our constraints as well as  $\Delta < 0.1, \alpha_D < 0.1$  and  $M_V \sim 3M_{\chi_1}$  (a) and  $M_V \sim 10M_{\chi_1}$  (b). Since the bound is weaker for smaller  $\Delta$  and  $\alpha_D$ , the represented lines are the strongest possible bounds from the analysis of [56] for both sets of points.

constraints from BBN-related observables, one can search for the  $e^+e^-$  pair produced by the decay. The reach is then significantly stronger as we show in Fig. 7. However, their bounds depends significantly on  $\Delta$  and is rapidly not competitive for lower values.

In [56] the thermal value target was almost systematically excluded for dark matter masses in our range of interest, however the fact that the dark Higgs boson opens several new annihilation channels modifies strongly this prediction, as we show in Fig. 7. Furthermore, the presence of a light dark Higgs boson modifies even more significantly the phenomenology when  $M_{\chi_2} - M_{\chi_1} > M_S$ . Indeed, the structure of our Lagrangian (namely the possibility of different Yukawa couplings between the right-handed and left-handed part of the original dark matter Dirac field) allows for the unsuppressed decay  $\chi_2 \rightarrow \chi_1 S$ . Hence, in this particular regime, the previous search channel is no longer open, but should be replaced by a search for dark Higgs boson decay as described above. This production mechanism should however be orders of magnitude larger than the Higgstrahlung, as it proceeds completely on-shell, leading to much stronger bounds than the one from Fig. 6. Thus, it would be interesting to re-run the search presented in [56] (in particular by estimating upcoming bounds from BDX [25]) while including the effect of a light dark Higgs boson. We save this analysis for future work.

## 4.2 BBN constraints

Bounds on dark Higgs bosons from BBN can be surprisingly strong, limiting lifetime to be as small as 0.1 s for sub-GeV dark Higgs when mixing with the SM Higgs boson is considered, as shown in [28]. As we will show in this section, these constraints

will be mitigated in our case due to two factors. First, due to its small mass, the dark Higgs boson decays only leptonically during BBN, and second, the annihilation mechanisms for our  $U(1)_D$ -charged Higgs boson are significantly more effective than the one in [28], so that the metastable density of dark Higgs boson after freeze-out is orders of magnitude smaller.

The decay products of long lived particles like the dark Higgs boson during the evolution of the Universe can distort the agreement between the standard BBN predictions and experimental observations of primordial abundances of light nuclei, in particular  $^3\text{He}$  and D. However, the annihilation of dark Higgs bosons during freeze-out provides a mechanism for depletion that can in turn ameliorate this potential disagreement. The energy injections from the decay of such long lived particles can be at early or late time. Here, early time refers to the early stages of BBN when  $t \lesssim 10$  s, wherein decays from a long lived particle could affect the neutron to proton ratio,  $n/p$ , or the effective number of neutrino species,  $N_{\text{eff}}$ . Late time refers to the later stages of BBN when  $t \gtrsim 100$  s which affects the final primordial abundances of light nuclei. We shall discuss constraints from both early as well as late time energy injection from  $S$  decays.

First we consider constraints from energy injection at early time. In particular, hadronic decays of dark Higgs boson, like for example mesons, occurring in the early universe could significantly alter the  $n/p$  ratio. Similarly, the direct production of neutrons and protons through quarks and gluons when the dark Higgs boson is sufficiently heavy can also give rise to stringent constraints on the lifetime of the dark Higgs boson [71, 72, 73, 74, 29]. However, in our case we restrict the dark Higgs boson mass  $M_S$  to be less than the dimuon threshold. This also means that there are no hadronic modes available for the dark Higgs boson decay and the only possible decay mode involves electrons. As a result we avoid stringent constraints from hadronic injections and instead we concentrate on the effect of injection of electrons from  $S$  decay. The effect it can have on BBN can be constrained using the PLANCK measured value of  $N_{\text{eff}}$ . The definition of effective number of neutrino species assumes that the three neutrino species instantaneously decouple giving a definite neutrino-photon temperature ratio  $T_\nu/T_\gamma = (4/11)^{1/3}$ , so that

$$N_{\text{eff}} = N_\nu \left( \frac{T_\nu}{T_\gamma} \right)^4 \left( \frac{4}{11} \right)^{-4/3}, \quad (4.6)$$

where  $N_\nu = 3$  is the number of neutrino species. Since the energy injected by the  $S$  decays will lead to a reheating of the electron-photon bath with respect to the neutrinos, this decreases  $T_\nu/T_\gamma$ . And as can be seen from Eq. (4.6), this leads to a lowering of  $N_{\text{eff}}$ . We use the result obtained in ref. [28] where an approximate analytical approach was adopted to calculate  $N_{\text{eff}}$  assuming a neutrino decoupling temperature of 1.4 MeV. The  $2\sigma$  lower bound from PLANCK [75] requires  $N_{\text{eff}} > 2.71$ . We show in Fig. 8 the exclusion limit on dark Higgs boson lifetime,  $\tau_S$ , as a function of  $\Omega_S h^2$ , the relic density the dark Higgs boson would have had today if it was stable. We see that most of the parameter space survives as a result of efficient annihilation channels of dark Higgs boson, particularly when  $M_S > M_\chi$  and the dark Higgs boson can annihilate into dark matter thereby decreasing its abundance substantially. However, when  $M_S < M_\chi$  this annihilation channel is not so efficient and the metastable abundance can be quite large and some of the parameter space especially above  $\tau \sim 100$  s is ruled out.

Next we consider the effect of late time energy injections at  $t \gtrsim 100$  s. Such late

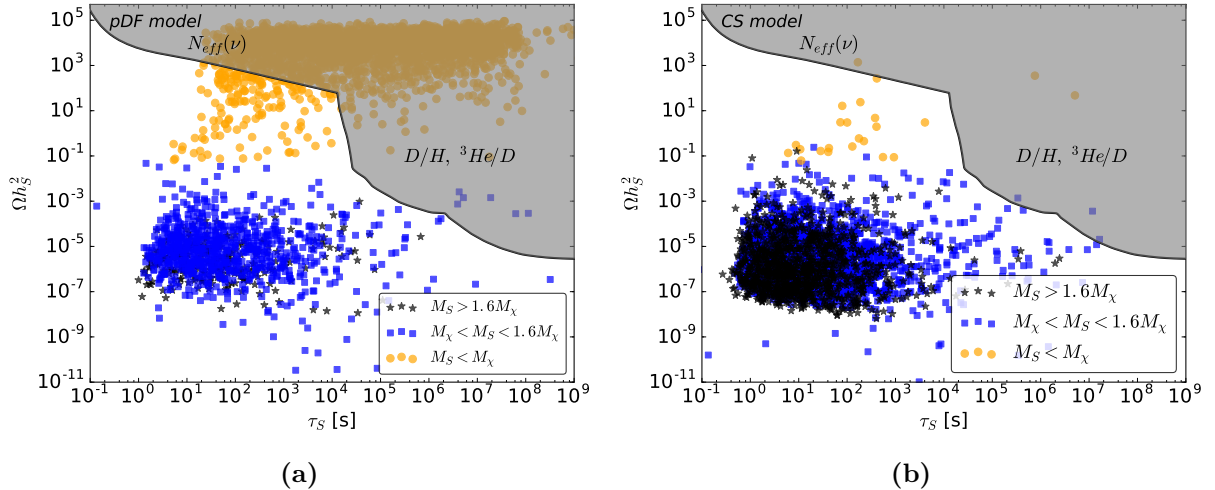


**Figure 8:** Constraints from light element abundances and from the effective number of neutrinos on the lifetime of the dark Higgs boson  $\tau_S$  and on its metastable relic density after freeze-out. In order to allow simple comparison with the dark matter relic density, we show the relic density  $\Omega h_S^2$  the dark Higgs boson would have had today if it was stable. Points satisfying the dark matter relic density constraint are overlaid for the *pDF* model (a) and for the *CS* case (b). The points have been sorted according to the mass range of the dark Higgs boson. Notice that CMB-related bounds are not included, which explain why points with  $M_S < M_\chi$  remain in the *CS* case.

energy injections can potentially destroy light nuclei through dissociation thereby altering their abundances. When the long lived particle primarily decays to hadrons the resulting hadro-dissociation can be very effective in reducing the primordial abundances even at relatively early times  $t \sim 100$  s. But once again in the dark Higgs boson scenario considered here the only viable decay mode is  $e^+e^-$  which leads to constraints only from electromagnetic showers. The absence of hadronic showers means that we avoid severe constraints from measurement of primordial abundances. The constraints from electromagnetic showers arise through photo-dissociation of light nuclei which become significant at  $t \gtrsim 10^4$  s. At  $t \sim 10^4 - 10^6$  s, the photo-dissociation of deuterium, while at  $t \gtrsim 10^6$  the over production of D and  ${}^3\text{He}$  through the photo-dissociation of  ${}^4\text{He}$  lead to the most stringent constraints [29]. The choice of parameters in this case as mentioned in the next section, leads to a lifetime in the range of  $1 - 10^5$  s. In this range of dark Higgs boson lifetime the bounds from  $N_{\text{eff}}$  are the most stringent up to  $\sim 10^4$  s, and above  $10^4$  s the bounds from D/H and  ${}^3\text{He}/\text{D}$  are the most stringent as far as BBN is concerned. In the dark Higgs boson scenario, however, there can be additional annihilation channels which can reduce the metastable abundance as mentioned in Sec. 3.1. For example, the production of a dark matter pair from dark Higgs boson annihilation can be significant for  $M_S \simeq M_\chi$ , thereby potentially avoiding constraints from BBN. In Fig. 8 we show the exclusion limits from D/H and  ${}^3\text{He}/\text{D}$  abundances. We see that most of the parameter space above  $10^4$  s is ruled out by these bounds, however one could still have substantial annihilation into dark matter which may allow a few points in the parameter space especially in the *pDF* case.

Bounds on the lifetime translate almost directly into a lower bound for the kinetic

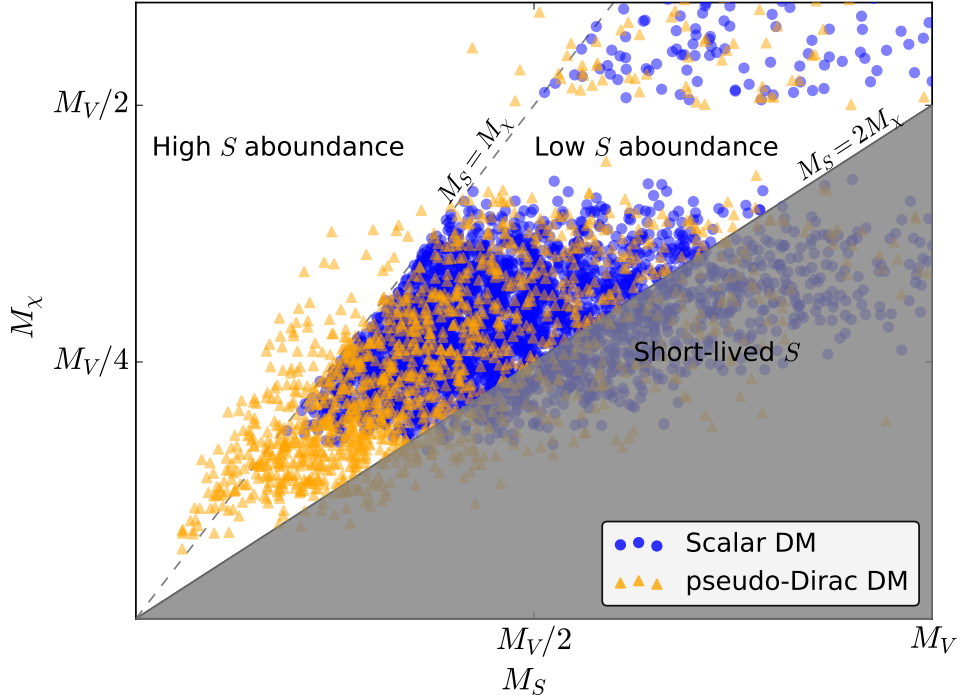


**Figure 9:** The four phenomenologically distinct regions described in the text shown in the dark matter mass  $M_\chi$  versus the dark Higgs boson mass  $M_S$  plane with data points from the  $CS$  case (blue) and the  $pDF$  case (orange) which satisfy all the constraints considered in this analysis. The grey-shaded regions mark the two regimes where the phenomenology does not significantly differ from previous studies.

mixing parameter from Eq. (2.12). When the dark Higgs boson metastable density is large as no effective annihilation into dark matter is possible, then we have the rough bound  $\varepsilon \gtrsim 10^{-4}$ . When  $M_S \gtrsim M_\chi$  the metastable density is suppressed by the annihilation process  $SS \rightarrow \chi\chi$  which dominates over the reverse process, and the bounds are significantly weakened. Most points still have  $\tau_S \lesssim 10^4$  s as can be seen in Fig. 8. However, this is not a strong bound and some more fine-tuned points can have longer lifetime, of order  $10^6$  s. For such high values of  $\tau_S$ , the mixing with the SM Higgs boson (which we neglected following the discussion of Sec. 2.2) should become competitive to mediate the dark Higgs boson decay.

## 5 Summary and conclusions

We have argued that in models with a massive, but light, dark vector mediator, the spectrum should naturally contain a light dark Higgs boson, whose presence can substantially modify the predictions of the two models considered in this paper. In the plane  $M_\chi - M_S$  we can identify four regions, as shown in Fig. 9, each with very distinct phenomenologies:

- The *secluded* regime ( $M_\chi \gtrsim M_V$ ) in which dark matter annihilation into  $VV$  becomes relevant. This tends to wash out the relic density for the value of the



dark gauge coupling considered, but is furthermore heavily constrained by CMB bounds as this is an  $s$ -wave process. We observed almost no points from our scans in this region.

- The *short-lived dark Higgs boson* regime corresponding to relatively heavy dark Higgs boson. This is the case considered in most of the previous literature, most notably recently in [56] for the  $pDF$  model. Dark Higgs bosons tend to decay instantaneously into a dark matter pair, leaving little new imprint, both in beam-dump experiments and in cosmological observables.
- The *long-lived dark Higgs boson* regime in which the dark Higgs boson is light enough so that it cannot decay into dark photon or dark matter particles. Its decay products can then be observed in beam-dump experiments, even though the corresponding bounds are often weaker than the missing energy searches by BaBar and NA64. Depending on whether or not one has  $M_S \lesssim M_\chi$ , this regime divides into two sub-regions:
  - The low abundance region,  $M_\chi < M_S < 2M_\chi$ , where the process  $SS \rightarrow \chi\chi$  is effective. The metastable density of dark Higgs bosons after freeze-out is therefore suppressed, so that the bounds from BBN are weakened.
  - The high abundance region,  $M_S < M_\chi$ , where there is no effective annihilation process for the dark Higgs boson. The consequent high metastable density of dark Higgs bosons translates into relatively strong bounds from BBN-related observables. Furthermore, the dark matter annihilation channel  $\chi\chi \rightarrow SS$  is kinematically open. Being an  $s$ -wave process for the model  $CS$ , this region is ruled out by CMB constraints, as can be seen in Fig. 9.

In Table 4, we give benchmark points for these regions satisfying all the constraints considered in this article.

In this paper, we have focused on the long-lived dark Higgs boson regime, as the secluded and short lived dark Higgs boson scenarios had already been covered extensively. We found that while the dark Higgs boson can in principle be produced and detected in proton beam-dump experiments, the thermal value target is out of reach of the experiments considered here. This conclusion should however be mitigated by several comments. First, as has been already advocated by many previous papers, it would be very interesting to make a re-analysis of the LSND data, possibly raising the energy threshold for the detected electrons and looking eventually for  $e^+e^-$  pair directly as this will significantly increase the reach of this experiment. Second, our conclusion regarding the reach of beam-dump experiments only applies to low-energy beam experiments, where the dominant production mechanism is meson decay. For more energetic beam experiments, or for electron beam dumps, different production channels for the dark Higgs boson, like direct production, should be considered. Finally, we expect that dark Higgs boson decay in proton beam-dump experiments could set stronger bounds than those of missing energy searches in the case of the  $pDF$  model when the process  $\chi_2 \rightarrow \chi_1 S$  is available.

On the other hand, the cosmology of the two models considered is significantly modified, with additional annihilation channels leading to various constraints. The bounds from the CMB arising from the fact that some of the new dark matter annihilation

Parameter	<i>pDF</i> model		<i>CS</i> model	
	Low $\Omega_S h^2$	High $\Omega_S h^2$	Low $\Omega_S h^2$	Short-lived S
$\lambda_S$	0.14	$1.8 \cdot 10^{-3}$	$1.35 \cdot 10^{-2}$	0.09
$g_V$	0.86	0.23	0.46	0.49
$M_V$	223	73	40	154
$\varepsilon$	$8.4 \cdot 10^{-4}$	$6.2 \cdot 10^{-4}$	$2.8 \cdot 10^{-4}$	$4 \cdot 10^{-5}$
$m_\chi$	47	15.1	12.6	58.6
$\lambda_{S\chi}$	–	–	$5.2 \cdot 10^{-3}$	0.016
$\lambda_\chi$	–	–	$1.8 \cdot 10^{-3}$	$4.4 \cdot 10^{-3}$
$y_{SL}$	0.013	$1.63 \cdot 10^{-3}$	–	–
$y_{SR}$	$6.2 \cdot 10^{-3}$	$2.1 \cdot 10^{-3}$	–	–
$M_S$	62.7	9.3	14.2	133
$M_\chi$	48.0	15.0	13.3	64.8
$\Omega_S h^2$	$3 \cdot 10^{-6}$	267	$0.7 \cdot 10^{-5}$	–
Dominant channels $\rightarrow$ relic density, $\langle\sigma v\rangle_{\text{an}}$	$e^+e^-$	$e^+e^-, SS$	$SS$	$e^+e^-$
$S$ lifetime (s)	2.7	101	436	–
NoE (LSND)	–	0.04	0.07	–
NoE (miniBooNE)	$1.1 \cdot 10^{-3}$	$6.8 \cdot 10^{-5}$	$0.14 \cdot 10^{-4}$	–
NoE (SBND)	0.094	$4.8 \cdot 10^{-3}$	$3.2 \cdot 10^{-4}$	–

**Table 4:** Benchmark points for the models analyzed in this work. Mass-related quantities are given in MeV and  $\text{MeV}^2$ , cross-section times velocity are in  $\text{cm}^3/\text{s}$ .

channels were unsuppressed at recombination time have been presented, excluding in particular completely the region  $M_\chi > M_S$  in the *CS* case. Furthermore, BBN-related observables which arise as a consequence of the long lifetime of the dark Higgs boson were found to be relevant, but weaker than could have been expected from previous works. We have summarized the main constraints on both the *CS* and *pDF* models in Fig. 10.

Regarding earth-based experiments, the most promising discovery channels for these models seem to be the missing-energy searches as they exclude already large portion of the parameter space. In the case of the *pDF* model, direct detection in beam-dump experiment of the decay of the heaviest dark matter field as advocated in [56] is a promising strategy which can be further combined with the search for dark Higgs boson from the  $\chi_2 \rightarrow \chi_1 S$  channel when it is kinematically accessible. It would be interesting to study other types of cosmological probes for an extremely long lived dark Higgs boson, as for example possible supernovae-related constraints or possible signatures from dark Higgs boson (or dark photon) production in DM annihilation in the sun as was already studied in [20, 76] for heavier dark matter candidates.

In the long run, the experimental prospects for both our models are bright. Almost



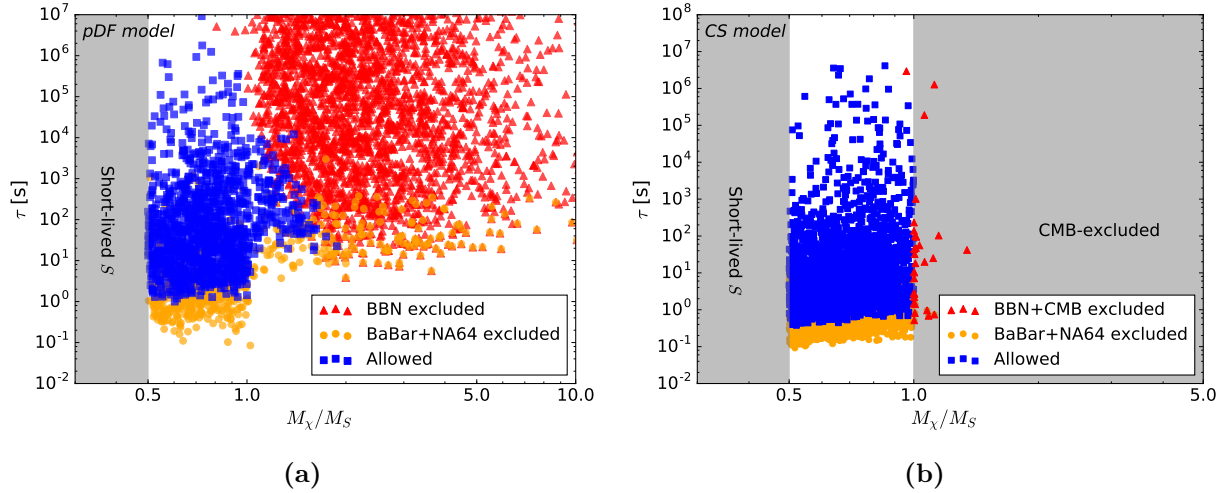


**Figure 10:** Summary of the various relevant bounds considered in this analysis, with the points satisfying the relic density constraint in the  $M_S/\tau_S$  plane for the  $pDF$  model **(a)** and the  $CS$  case **(b)** overlaid. We have restricted the points to the region of long-lived dark Higgs boson where the phenomenology is distinctively different from the previous studies of these models.

all of the parameter space which meets the thermal value target will be independently probed by the next generation of projected electron beam-dump experiments (for instance LDMX), by direct detection experiments such as XENON1T for the  $CS$  model, and by indirect detection experiments searching for current dark matter annihilation in the MeV mass range.

### Acknowledgments

The authors warmly thank Felix Kahlhoefer for pointing out an error in the estimation of the dark matter annihilation rates in the pre-print version of this paper. LD and SR would like to thank P. deNiverville for helpful discussions regarding his code BdNMC. LR is supported by the Lancaster-Manchester-Sheffield Consortium for Fundamental Physics under STFC Grant No. ST/L000520/1. LD, LR and SR are supported in part by the National Science Council (NCN) research grant No. 2015-18-A-ST2-00748. The use of the CIS computer cluster at the National Centre for Nuclear Research in Warsaw is gratefully acknowledged.

# A Differential production rate of dark Higgs boson from meson decay

We present in this appendix more details about the differential cross-section corresponding to the three-body scalar meson decays into a photon, a dark photon and a dark Higgs boson (see Fig. 4).

We associate the four-momentum  $p$  to the outgoing photon,  $q$  to the excited intermediary dark photon and  $k$  the outgoing dark photon. The coupling  $c_S$  between a dark Higgs boson and two dark photons is given with our parameter by

$$c_s = g_V^2 q_S^2 v_S ,$$

where  $q_S$  is the dark Higgs boson charge. We use the usual notation  $s = q^\mu q_\mu$  and denote the photon (dark photon) polarization four-vector by  $\mathbf{e}^\mu$  ( $\tilde{\mathbf{e}}^\mu$ ). Following [77] we can then write the amplitude for this process from the one giving the decay of meson into two photons mediated by the chiral anomaly as

$$\mathcal{A}_{M \rightarrow \gamma SV} = \frac{\varepsilon \alpha_{em}}{\pi f_\pi} (2c_S) \varepsilon^{\mu\nu\alpha\beta} p_\alpha q_\beta \mathbf{e}_\mu \tilde{\mathbf{e}}_\lambda^* \frac{\delta_\nu^\lambda - q_\nu q^\lambda / M_V^2}{(s - M_V^2) + i M_V \Gamma_V} , \quad (\text{A.1})$$

where we have used the factor  $f_\pi$  defined from the decay width of the meson into a pair of photons as

$$\Gamma_{M \rightarrow \gamma\gamma} \equiv \frac{1}{f_\pi^2} \frac{\alpha_{em}^2 m_M^3}{(4\pi)^3} . \quad (\text{A.2})$$

Using the following useful kinematic relations:

$$\begin{aligned} p^2 &= 0 , & q^2 &= s , & k^2 &= M_V^2 , \\ k \cdot q &= \frac{s + M_V^2 - M_S^2}{2} , & p \cdot q &= \frac{m_M^2 - s}{2} , \end{aligned}$$

we can then square the amplitude and sum over the outgoing polarization states. We obtain

$$\begin{aligned} \langle |\mathcal{A}_{M \rightarrow \gamma SV}|^2 \rangle &= \frac{\varepsilon^2 \alpha_{em}^2 c_S^2}{4\pi^2 f_\pi^2} \frac{1}{(s - M_V^2)^2 + M_V^2 \Gamma_V^2} \\ &\quad \left[ \frac{(m_M^2 - s)^2}{4} - \frac{p \cdot k}{M_V^2} \left( s(p \cdot k) - (m_M^2 - s) \frac{s + M_V^2 - M_S^2}{2} \right) \right] . \end{aligned} \quad (\text{A.3})$$

Introducing the angle  $\theta$  between the outgoing dark Higgs boson and the excited dark photon direction, chosen in the rest frame of the excited dark photon, we can expand  $(p \cdot k)$  as

$$p \cdot k = \frac{1}{4s} (m_M^2 - s) \left[ (s + M_V^2 - M_S^2) + \sqrt{\lambda(s, M_V^2, M_S^2)} \cos \theta \right] ,$$

where we have used the usual definition for the kinematic triangle function  $\lambda$ :

$$\lambda(a, b, c) = a^2 + b^2 + c^2 - 2ab - 2ac - 2bc .$$

In order to simulate the decay chains in our Monte-Carlo simulation, we need the differential branching ratio  $\frac{d^2\text{BR}_{M\rightarrow\gamma SV}}{dsd\theta}$ . Writing the two-body phase space differential element  $d\Pi^2$ , we can use the recursion relations to decompose the three-body phase space into two-body ones combined with an extra integral over the excited dark photon squared momentum  $s$ , leading to

$$\text{BR}_{M\rightarrow\gamma SV} = \frac{1}{2m_M\Gamma_M} \int \frac{ds}{2\pi} d\Pi_{M\rightarrow\gamma V^*} d\Pi_{V^*\rightarrow VS} \langle |\mathcal{A}_{M\rightarrow\gamma SV}|^2 \rangle, \quad (\text{A.4})$$

with the integration on  $s$  running between  $(M_V + M_S)^2$  and  $m_M^2$ . Integrating directly on  $d\Pi_{M\rightarrow\gamma V^*}$  and on every angle but  $\theta$ , we have

$$\int d\Pi_{M\rightarrow\gamma V^*} d\Pi_{V^*\rightarrow VS} \longrightarrow \int (d\theta \sin\theta) \frac{1}{128\pi^2} \left(1 - \frac{s}{m_M^2}\right) \frac{\sqrt{\lambda(s, M_V^2, M_S^2)}}{s}. \quad (\text{A.5})$$

Finally, using the definition of  $M_V \equiv v_S g_V q_S$ , we can combined Eq. (A.3) and Eq. (A.5) to get our result

$$\frac{d^2\text{BR}_{M\rightarrow\gamma SV}}{dsd\theta} = \text{BR}_{M\rightarrow\gamma\gamma} \times \frac{\varepsilon^2 \alpha_D q_S^2}{8\pi} s \left(1 - \frac{s}{m_{\pi_0}^2}\right)^6 \times \frac{\sqrt{\lambda} (8M_V^2/s + \lambda \sin^2\theta)}{(s - M_V^2)^2 + M_V^2 \Gamma_V^2} \sin\theta, \quad (\text{A.6})$$

where we used the short-hand notation  $\lambda \equiv \lambda(1, M_V^2/s, M_S^2/s)$ .

## References

- [1] L. Roszkowski, E. M. Sessolo, and S. Trojanowski, “WIMP dark matter candidates and searches - current issues and future prospects,” [arXiv:1707.06277 \[hep-ph\]](#).
- [2] T. Plehn, “Yet Another Introduction to Dark Matter,” [arXiv:1705.01987 \[hep-ph\]](#).
- [3] M. Battaglieri *et al.*, “US Cosmic Visions: New Ideas in Dark Matter 2017: Community Report,” *FERMILAB-CONF-17-282-AE-PPD-T* (2017) , [arXiv:1707.04591 \[hep-ph\]](#).
- [4] J. Alexander *et al.*, “Dark Sectors 2016 Workshop: Community Report,” *FERMILAB-CONF-16-421* (2016) , [arXiv:1608.08632 \[hep-ph\]](#).
- [5] X. Chu, C. Garcia-Cely, and T. Hambye, “Can the relic density of self-interacting dark matter be due to annihilations into Standard Model particles?,” *JHEP* **11** (2016) 048, [arXiv:1609.00399 \[hep-ph\]](#).
- [6] F. C. Correia and S. Fajfer, “Restrained dark  $U(1)_d$  at low energies,” *Phys. Rev.* **D94** no. 11, (2016) 115023, [arXiv:1609.00860 \[hep-ph\]](#).
- [7] S. Knapen, T. Lin, and K. M. Zurek, “Light Dark Matter: Models and Constraints,” [arXiv:1709.07882 \[hep-ph\]](#).
- [8] E. Kuflik, M. Perelstein, N. R.-L. Lorier, and Y.-D. Tsai, “Phenomenology of ELDER Dark Matter,” *JHEP* **08** (2017) 078, [arXiv:1706.05381 \[hep-ph\]](#).
- [9] J. L. Feng and J. Smolinsky, “Impact of Resonance on Thermal Targets for Invisible Dark Photon Searches,” [arXiv:1707.03835 \[hep-ph\]](#).
- [10] M. Duch, B. Grzadkowski, and D. Huang, “Strongly self-interacting vector dark matter via freeze-in,” [arXiv:1710.00320 \[hep-ph\]](#).
- [11] J. L. Feng, I. Galon, F. Kling, and S. Trojanowski, “Dark Higgs Bosons at FASER,” [arXiv:1710.09387 \[hep-ph\]](#).
- [12] B. Wojtsekhowski *et al.*, “Searching for a dark photon: Project of the experiment at VEPP-3,” [arXiv:1708.07901 \[hep-ex\]](#).
- [13] J. Feng, I. Galon, F. Kling, and S. Trojanowski, “FASER: ForwArd Search ExpeRiment at the LHC,” [arXiv:1708.09389 \[hep-ph\]](#).
- [14] S. Tulin and H.-B. Yu, “Dark Matter Self-interactions and Small Scale Structure,” [arXiv:1705.02358 \[hep-ph\]](#).
- [15] D. E. Morrissey and A. P. Spray, “New Limits on Light Hidden Sectors from Fixed-Target Experiments,” *JHEP* **06** (2014) 083, [arXiv:1402.4817 \[hep-ph\]](#).
- [16] D. Feldman, Z. Liu, and P. Nath, “The Stueckelberg Z-prime Extension with Kinetic Mixing and Milli-Charged Dark Matter From the Hidden Sector,” *Phys. Rev.* **D75** (2007) 115001, [arXiv:hep-ph/0702123 \[HEP-PH\]](#).
- [17] S.-M. Choi, Y.-J. Kang, and H. M. Lee, “On thermal production of self-interacting dark matter,” *JHEP* **12** (2016) 099, [arXiv:1610.04748 \[hep-ph\]](#).

- [18] B. Batell, M. Pospelov, and A. Ritz, “Exploring Portals to a Hidden Sector Through Fixed Targets,” *Phys. Rev.* **D80** (2009) 095024, [arXiv:0906.5614 \[hep-ph\]](#).
- [19] J. D. Bjorken, R. Essig, P. Schuster, and N. Toro, “New Fixed-Target Experiments to Search for Dark Gauge Forces,” *Phys. Rev.* **D80** (2009) 075018, [arXiv:0906.0580 \[hep-ph\]](#).
- [20] P. Schuster, N. Toro, and I. Yavin, “Terrestrial and Solar Limits on Long-Lived Particles in a Dark Sector,” *Phys. Rev.* **D81** (2010) 016002, [arXiv:0910.1602 \[hep-ph\]](#).
- [21] R. Essig, P. Schuster, and N. Toro, “Probing Dark Forces and Light Hidden Sectors at Low-Energy e+e- Colliders,” *Phys. Rev.* **D80** (2009) 015003, [arXiv:0903.3941 \[hep-ph\]](#).
- [22] B. Batell, R. Essig, and Z. Surujon, “Strong Constraints on Sub-GeV Dark Sectors from SLAC Beam Dump E137,” *Phys. Rev. Lett.* **113** no. 17, (2014) 171802, [arXiv:1406.2698 \[hep-ph\]](#).
- [23] E. Izaguirre, G. Krnjaic, P. Schuster, and N. Toro, “Analyzing the Discovery Potential for Light Dark Matter,” *Phys. Rev. Lett.* **115** no. 25, (2015) 251301, [arXiv:1505.00011 \[hep-ph\]](#).
- [24] P. deNiverville, C.-Y. Chen, M. Pospelov, and A. Ritz, “Light dark matter in neutrino beams: production modelling and scattering signatures at MiniBooNE, T2K and SHiP,” *Phys. Rev.* **D95** no. 3, (2017) 035006, [arXiv:1609.01770 \[hep-ph\]](#).
- [25] **BDX** Collaboration, M. Battaglieri *et al.*, “Dark Matter Search in a Beam-Dump eXperiment (BDX) at Jefferson Lab,” [arXiv:1607.01390 \[hep-ex\]](#).
- [26] T. R. Slatyer, “Indirect dark matter signatures in the cosmic dark ages. I. Generalizing the bound on s-wave dark matter annihilation from Planck results,” *Phys. Rev.* **D93** no. 2, (2016) 023527, [arXiv:1506.03811 \[hep-ph\]](#).
- [27] H. Liu, T. R. Slatyer, and J. Zavala, “Contributions to cosmic reionization from dark matter annihilation and decay,” *Phys. Rev.* **D94** no. 6, (2016) 063507, [arXiv:1604.02457 \[astro-ph.CO\]](#).
- [28] A. Fradette and M. Pospelov, “BBN for the LHC: constraints on lifetimes of the Higgs portal scalars,” [arXiv:1706.01920 \[hep-ph\]](#).
- [29] M. Kawasaki, K. Kohri, T. Moroi, and Y. Takaesu, “Revisiting Big-Bang Nucleosynthesis Constraints on Long-Lived Decaying Particles,” [arXiv:1709.01211 \[hep-ph\]](#).
- [30] B. Holdom, “Two U(1)’s and Epsilon Charge Shifts,” *Phys. Lett.* **166B** (1986) 196–198.
- [31] J. Berger, K. Jedamzik, and D. G. E. Walker, “Cosmological Constraints on Decoupled Dark Photons and Dark Higgs,” *JCAP* **1611** (2016) 032, [arXiv:1605.07195 \[hep-ph\]](#).
- [32] B. Batell, M. Pospelov, and A. Ritz, “Probing a Secluded U(1) at B-factories,” *Phys. Rev.* **D79** (2009) 115008, [arXiv:0903.0363 \[hep-ph\]](#).

- [33] **NA48/2** Collaboration, J. R. Batley *et al.*, “Search for the dark photon in  $\pi^0$  decays,” *Phys. Lett.* **B746** (2015) 178–185, [arXiv:1504.00607 \[hep-ex\]](#).
- [34] **BaBar** Collaboration, J. P. Lees *et al.*, “Search for a Dark Photon in  $e^+e^-$  Collisions at BaBar,” *Phys. Rev. Lett.* **113** no. 20, (2014) 201801, [arXiv:1406.2980 \[hep-ex\]](#).
- [35] **LHCb** Collaboration, R. Aaij *et al.*, “Search for dark photons produced in 13 TeV  $pp$  collisions,” [arXiv:1710.02867 \[hep-ex\]](#).
- [36] S. Andreas *et al.*, “Proposal for an Experiment to Search for Light Dark Matter at the SPS,” [arXiv:1312.3309 \[hep-ex\]](#).
- [37] E. Izaguirre, G. Krnjaic, P. Schuster, and N. Toro, “Testing GeV-Scale Dark Matter with Fixed-Target Missing Momentum Experiments,” *Phys. Rev.* **D91** no. 9, (2015) 094026, [arXiv:1411.1404 \[hep-ph\]](#).
- [38] **BaBar** Collaboration, J. P. Lees *et al.*, “Search for Invisible Decays of a Dark Photon Produced in  $e^+e^-$  Collisions at BaBar,” *Phys. Rev. Lett.* **119** no. 13, (2017) 131804, [arXiv:1702.03327 \[hep-ex\]](#).
- [39] **NA64** Collaboration, D. Banerjee *et al.*, “Search for vector mediator of Dark Matter production in invisible decay mode,” [arXiv:1710.00971 \[hep-ex\]](#).
- [40] F. Feroz, M. P. Hobson, and M. Bridges, “MultiNest: an efficient and robust Bayesian inference tool for cosmology and particle physics,” *Mon. Not. Roy. Astron. Soc.* **398** (2009) 1601–1614, [arXiv:0809.3437 \[astro-ph\]](#).
- [41] **Planck** Collaboration, P. A. R. Ade *et al.*, “Planck 2015 results. XIII. Cosmological parameters,” *Astron. Astrophys.* **594** (2016) A13, [arXiv:1502.01589 \[astro-ph.CO\]](#).
- [42] G. Blanger, F. Boudjema, A. Pukhov, and A. Semenov, “micrOMEGAs4.1: two dark matter candidates,” *Comput. Phys. Commun.* **192** (2015) 322–329, [arXiv:1407.6129 \[hep-ph\]](#).
- [43] W. Porod, “SPHeno, a program for calculating supersymmetric spectra, SUSY particle decays and SUSY particle production at  $e^+e^-$  colliders,” *Comput. Phys. Commun.* **153** (2003) 275–315, [arXiv:hep-ph/0301101 \[hep-ph\]](#).
- [44] W. Porod and F. Staub, “SPHeno 3.1: Extensions including flavour, CP-phases and models beyond the MSSM,” *Comput. Phys. Commun.* **183** (2012) 2458–2469, [arXiv:1104.1573 \[hep-ph\]](#).
- [45] F. Staub, “SARAH,” [arXiv:0806.0538 \[hep-ph\]](#).
- [46] F. Staub, “SARAH 3.2: Dirac Gauginos, UFO output, and more,” *Comput. Phys. Commun.* **184** (2013) 1792–1809, [arXiv:1207.0906 \[hep-ph\]](#).
- [47] F. Staub, “SARAH 4 : A tool for (not only SUSY) model builders,” *Comput. Phys. Commun.* **185** (2014) 1773–1790, [arXiv:1309.7223 \[hep-ph\]](#).
- [48] J. Liu, N. Weiner, and W. Xue, “Signals of a Light Dark Force in the Galactic Center,” *JHEP* **08** (2015) 050, [arXiv:1412.1485 \[hep-ph\]](#).
- [49] P. Gondolo and G. Gelmini, “Cosmic abundances of stable particles: Improved analysis,” *Nucl. Phys.* **B360** (1991) 145–179.

- [50] E. W. Kolb and M. S. Turner, “The Early Universe,” *Front. Phys.* **69** (1990) 1–547.
- [51] C. Boehm and P. Fayet, “Scalar dark matter candidates,” *Nucl. Phys.* **B683** (2004) 219–263, [arXiv:hep-ph/0305261 \[hep-ph\]](#).
- [52] P. deNiverville, M. Pospelov, and A. Ritz, “Observing a light dark matter beam with neutrino experiments,” *Phys. Rev.* **D84** (2011) 075020, [arXiv:1107.4580 \[hep-ph\]](#).
- [53] M. Pospelov, A. Ritz, and M. B. Voloshin, “Secluded WIMP Dark Matter,” *Phys. Lett.* **B662** (2008) 53–61, [arXiv:0711.4866 \[hep-ph\]](#).
- [54] C. Kouvaris, I. M. Shoemaker, and K. Tuominen, “Self-Interacting Dark Matter through the Higgs Portal,” *Phys. Rev.* **D91** no. 4, (2015) 043519, [arXiv:1411.3730 \[hep-ph\]](#).
- [55] G. Krnjaic, “Probing Light Thermal Dark-Matter With a Higgs Portal Mediator,” *Phys. Rev.* **D94** no. 7, (2016) 073009, [arXiv:1512.04119 \[hep-ph\]](#).
- [56] E. Izaguirre, Y. Kahn, G. Krnjaic, and M. Moschella, “Testing Light Dark Matter Coannihilation With Fixed-Target Experiments,” *Phys. Rev.* **D96** no. 5, (2017) 055007, [arXiv:1703.06881 \[hep-ph\]](#).
- [57] K. M. Nollett and G. Steigman, “BBN And The CMB Constrain Light, Electromagnetically Coupled WIMPs,” *Phys. Rev.* **D89** no. 8, (2014) 083508, [arXiv:1312.5725 \[astro-ph.CO\]](#).
- [58] J. Tiffenberg, M. Sofo-Haro, A. Drlica-Wagner, R. Essig, Y. Guardincerri, S. Holland, T. Volansky, and T.-T. Yu, “Single-electron and single-photon sensitivity with a silicon Skipper CCD,” *Phys. Rev. Lett.* **119** no. 13, (2017) 131802, [arXiv:1706.00028 \[physics.ins-det\]](#).
- [59] R. Essig, T. Volansky, and T.-T. Yu, “New Constraints and Prospects for sub-GeV Dark Matter Scattering off Electrons in Xenon,” *Phys. Rev.* **D96** no. 4, (2017) 043017, [arXiv:1703.00910 \[hep-ph\]](#).
- [60] R. Essig, A. Manalaysay, J. Mardon, P. Sorensen, and T. Volansky, “First Direct Detection Limits on sub-GeV Dark Matter from XENON10,” *Phys. Rev. Lett.* **109** (2012) 021301, [arXiv:1206.2644 \[astro-ph.CO\]](#).
- [61] M. Kaplinghat, S. Tulin, and H.-B. Yu, “Direct Detection Portals for Self-interacting Dark Matter,” *Phys. Rev.* **D89** no. 3, (2014) 035009, [arXiv:1310.7945 \[hep-ph\]](#).
- [62] **LSND** Collaboration, C. Athanassopoulos *et al.*, “The Liquid scintillator neutrino detector and LAMPF neutrino source,” *Nucl. Instrum. Meth.* **A388** (1997) 149–172, [arXiv:nucl-ex/9605002 \[nucl-ex\]](#).
- [63] **MiniBooNE** Collaboration, A. A. Aguilar-Arevalo *et al.*, “The MiniBooNE Detector,” *Nucl. Instrum. Meth.* **A599** (2009) 28–46, [arXiv:0806.4201 \[hep-ex\]](#).
- [64] **LAr1-ND, ICARUS-WA104, MicroBooNE** Collaboration, M. Antonello *et al.*, “A Proposal for a Three Detector Short-Baseline Neutrino Oscillation Program in the Fermilab Booster Neutrino Beam,” [arXiv:1503.01520 \[physics.ins-det\]](#).



- [65] E. M. Riordan *et al.*, “A Search for Short Lived Axions in an Electron Beam Dump Experiment,” *Phys. Rev. Lett.* **59** (1987) 755.
- [66] B. Batell, P. deNiverville, D. McKeen, M. Pospelov, and A. Ritz, “Leptophobic Dark Matter at Neutrino Factories,” *Phys. Rev.* **D90** no. 11, (2014) 115014, [arXiv:1405.7049 \[hep-ph\]](#).
- [67] **LSND** Collaboration, C. Athanassopoulos *et al.*, “Evidence for muon-neutrino  $\rightarrow$  electron-neutrino oscillations from pion decay in flight neutrinos,” *Phys. Rev.* **C58** (1998) 2489–2511, [arXiv:nucl-ex/9706006 \[nucl-ex\]](#).
- [68] **LSND** Collaboration, A. Aguilar-Arevalo *et al.*, “Evidence for neutrino oscillations from the observation of anti-neutrino(electron) appearance in a anti-neutrino(muon) beam,” *Phys. Rev.* **D64** (2001) 112007, [arXiv:hep-ex/0104049 \[hep-ex\]](#).
- [69] **MiniBooNE** Collaboration, A. A. Aguilar-Arevalo *et al.*, “Dark Matter Search in a Proton Beam Dump with MiniBooNE,” *Phys. Rev. Lett.* **118** no. 22, (2017) 221803, [arXiv:1702.02688 \[hep-ex\]](#).
- [70] R. B. Patterson, E. M. Laird, Y. Liu, P. D. Meyers, I. Stancu, and H. A. Tanaka, “The Extended-track reconstruction for MiniBooNE,” *Nucl. Instrum. Meth.* **A608** (2009) 206–224, [arXiv:0902.2222 \[hep-ex\]](#).
- [71] R. H. Cyburt, J. R. Ellis, B. D. Fields, and K. A. Olive, “Updated nucleosynthesis constraints on unstable relic particles,” *Phys. Rev.* **D67** (2003) 103521, [arXiv:astro-ph/0211258 \[astro-ph\]](#).
- [72] M. Kawasaki, K. Kohri, and T. Moroi, “Hadronic decay of late - decaying particles and Big-Bang Nucleosynthesis,” *Phys. Lett.* **B625** (2005) 7–12, [arXiv:astro-ph/0402490 \[astro-ph\]](#).
- [73] K. Jedamzik, “Big bang nucleosynthesis constraints on hadronically and electromagnetically decaying relic neutral particles,” *Phys. Rev.* **D74** (2006) 103509, [arXiv:hep-ph/0604251 \[hep-ph\]](#).
- [74] M. Pospelov and J. Pradler, “Big Bang Nucleosynthesis as a Probe of New Physics,” *Ann. Rev. Nucl. Part. Sci.* **60** (2010) 539–568, [arXiv:1011.1054 \[hep-ph\]](#).
- [75] **Planck** Collaboration, P. A. R. Ade *et al.*, “Planck 2015 results. XIII. Cosmological parameters,” *Astron. Astrophys.* **594** (2016) A13, [arXiv:1502.01589 \[astro-ph.CO\]](#).
- [76] J. Smolinsky and P. Tanedo, “Dark Photons from Captured Inelastic Dark Matter Annihilation: Charged Particle Signatures,” *Phys. Rev.* **D95** no. 7, (2017) 075015, [arXiv:1701.03168 \[hep-ph\]](#).
- [77] Y. Kahn, G. Krnjaic, J. Thaler, and M. Toups, “DAEALUS and dark matter detection,” *Phys. Rev.* **D91** no. 5, (2015) 055006, [arXiv:1411.1055 \[hep-ph\]](#).